Pantothenate Kinase 4 Governs Lens Epithelial Fibrosis by Negatively Regulating PKM2 Related Glycolysis

Xue Li [1], Lin-Lin Luo [1], Qiu-Mei Hu [1], Xi Chen [1], Rui-Feng Li [1], Chun-Lin Chen [1], Min Sun [1]*, Sen Lin [2]*

[1]Department of Ophthalmology, Daping Hospital, Army Medical Center of PLA, Army Medical University, Chongqing, 400042

[2]Department of Neurology, Xinqiao Hospital, The Second Affiliated Hospital, Army Medical University, Chongqing, 400037

Corresponding authors: Lin Sen, sam_lin_amc@163.com; Sun Min, minmins@126.com

Key words: PANK4; Fibrosis; Lens epithelial cell; Epithelial-Mesenchymal Transition; PKM2; Glycolysis; HIF

Abstract

Lens fibrosis is one of the leading causes of cataract. Though the epithelial-mesenchymal transition (EMT) causes anterior subcapsular cataract (ASC) and posterior capsule opacification (PCO) which could be eliminated by surgery, yet lacks effective drug, and the mechanism elucidation which may shed on light on other organ fibrosis treatment. In current study, we discovered a novel mechanism that regulate lens epithelial cell (LEC) EMT. Firstly, pantothenate kinase 4 (PANK4) level is corelated with aging in cataract patients and mice. Loss of function of PANK4 significantly contribute to alleviate the EMT of LECs by upregulating PKM2 which was phosphorylated at Y105 residue thus switching oxidative phosphorylation to glycolysis. However, PKM2 regulation did not affect PANK4 which demonstrate the downstream role of PKM2. Inhibition of PKM2 in *Pank4*$^{-/-}$ mice cause lens fibrosis, which strengthen the results that PANK4-PKM2 axis is required for LEC EMT. It was also found glycolytic governed HIF signaling involves in the PANK4-PKM2 related downstream signaling. However, HIF-1 elevation is independent of PKM2(S37) but Y105 residue when PANK4 deleted, which demonstrated PKM2 and HIF-1 not involve in a classic positive feedback loop. Collectively, these results indicated a novel PANK4 related glycolysis switch which may contribute to HIF-1 stabilization and PKM2 phosphorylation at Y105, and inhibit the LEC EMT process.

Introduction

Lens fibrosis, which is characterized by hyperproliferation, migration, and the epithelial–mesenchymal transition (EMT) of LECs, cause anterior subcapsular cataract (ASC) and posterior capsule opacification (PCO) insulting the vision by changing light scattering[1]. Because the unique biological properties of lens, it could act as an ideal model for investigating the molecular mechanisms of tissue and organ fibrosis, such as liver cirrhosis, idiopathic pulmonary fibrosis and renal fibrosis, which account for more than 45% mortality[2, 3]. EMT is a major cause of the progression in organ fibrosis and ocular fibrosis, including several eye diseases, including PCO, ASC, pterygium, and glaucoma, and is part of the wound-healing process post-ocular surgery[4-9]. In fibrotic cataract, lens epithelium loss their integrity and normal function but disorganized with excessive fibronectin (FN) and collagen (Col) in extracellular matrix (ECM). When transition of epithelial-to-mesenchymal starts, the EMT of lens epithelium was regulated by varieties of mechanisms with the classic prominent roles of Transforming growth factor (TGFβ)/Smad signaling[10-13] and glycolytic metabolism[14]. The lens is an avascular tissue relying on limited supply of oxygen and glucose[15] and lens epithelium can utilize oxidative phosphorylation (OXPHOS) for the generation of ATP by mitochondria, however, the lens fiber cells are reliant on the glycolysis to support their energy demands[14]. Hence, the regulation of glycolytic metabolism of LECs would be a potential strategy to prevent lens fibrosis. However, publications on the relationship of cataract to statins (HMG-CoA reductase inhibitors) have reported inconsistent findings[16-18]. Acetyl-CoA is the precursor to HMG-CoA, one of the products of CoA which is produced during the second step of aerobic cellular respiration, pyruvate decarboxylation, occurs in the matrix of the mitochondria. PANK1, PANK2 and PANK3 are key regulatory enzymes involved in the CoA biosynthetic pathway[19], which catalyze the phosphorylation of the vitamin pantothenate to 4'-phosphopantothenate, subsequently leads to the formation of CoA. However, the fourth member of PANK family, PANK4, lacks enzyme activity because it misses an important catalytic glutamate site and its name is thus a misnomer[19-21]. In previous study, we found a novel PANK4 mutation in congenital cataract formation[22], which results in the apoptosis of lens epithelial cells and the aberrant expression patterns of crystallin. Yet, the function and mechanism of PANK4 is still under consideration.

Studies in Han Chinese have indeed shown that gene polymorphisms in PANK4 are associated with type 2 diabetes[23] and functional experiments have shown that PANK4 can affect the apoptosis of pancreatic β cells[24]. In diabetic cataract formation, aldose reductase (AR) mediated polyol accumulation has been shown to lead to EMT, characterized by osmotic imbalances and oxidative stress that result in fiber cell swelling, liquefaction and eventually development of cataracts[25, 26] [27]. Eventually, the AR leads to the formation of pyruvate generation which is limited by pyruvate

kinase M2 isozyme (PKM2) in the last step of glycolysis [28, 29]. It was indicated rat Pank4 was found to be associated with PKM2 with KOG2201 and KOG4584 domain under both in vitro and in vivo conditions[30]. PKM2 was previously reported expressed in fetal tissues and cancers, and has been shown to be part of EMT in human colorectal cancer cells[31]. PKM2 expression is enhanced in cancers and favors the glycolytic pathway and potentially the metastatic potential such as in pancreatic ductal adenocarcinoma tissues and cell lines[32]. PKM2-mediated glycolysis also involved in inflammasome activation by modulating EIF2AK2 phosphorylation in macrophages[33]. Moreover, activation of PKM2 is a potentiate treatment against diabetic nephropathy by increasing the glucose metabolic flux and inhibiting the production of toxic glucose metabolites[34]. PKM2 is recruited to phosphorylate histone H3 at T11 which results in H3-K9 acetylation and transcription of glycolytic genes including *GLUT1, MYC, CCND1,* lactate dehydrogenase A (*LDHA*) that enhancing the Warburg effect, whereas PKM2 is reported as a substrate of Cdc25A which formed a positive feedback loop[35-38]. Unlike many other organs, lens grows throughout our life although at a slow rate in adult lenses compared to the young lenses depending on glycolic activities [39]. However, is it unclear whether PKM2 dependent glycolic metabolism maybe one of the major activities in lens epithelium maintenance and in lens epithelium EMT process. Nonetheless, the relationship of PANK4 and PKM2 in cataract and lens epithelium metabolism remain unclear.

In current study, we investigated a role of PANK4 in lens epithelium EMT and fibrosis. We show that PANK4 specifically expressed in human and mice lens epithelium, which negatively regulates the LEC EMT process and functions in a PKM2 phosphorylation depending glycolytic metabolism manner. Without PANK4, the aging and injury related lens epithelium fibrosis are attenuated. Meanwhile, the glycolytic metabolism balance is perturbed. The suppression of the metabolic switch in LEC through PKM2 activation or by PANK4 loss of function speeds the EMT of the LECs. In contrast, preemptive amplification of the metabolic response through inhibition of PKM2 confers the promotion of lens epithelium EMT process, which shed light on the potentiation of clinical drugs in preventing the PCO formation.

Materials and Methods

Pank4 transgenic mice generation

Pank4$^{-/-}$ mice were generated by Nanjing Biomedical Research Institute of Nanjing University, China, similar as previously described, with 5bp mutation [40]. Briefly, we made *pank4* knockout mice via the CRISPR/Cas9 system. Cas9 mRNA and sgRNA were co-injected into zygotes. sgRNA direct Cas9 endonuclease caused a cleavage in exon3, and creates a double-strand break (DSB). Such breaks will be repaired by non-homologous end jointing (NHEJ), and result in destruction of the *Pank4* gene. The

Pank4 targeting sequence is *gacgtggagcaggatcatgagccaccctatgagatctcagtccaggag agatcacagctcgcctgcatttcatcaagtttgagaatacctacatggaagcctgcctggacttcatcagagaccaccta gtcaacactgagaccaaggtcatccaggccactgggggtggagcctacaagttcaaggacctcatcgaggagaagc tgcgtctgaa*. Offspring were screened for correct genotype by PCR analysis of tail DNA. Mice were housed in cages in a room with a 12-hr light-dark cycle with ad libitum access to water and rodent chow diet. Animal protocols have been approved by the Institutional Animal Care and Use Committee (IACUC) of Army Medical Center, Army Medical University (No. AMUWEC20201055).

Lens capsular injury induced fibrosis model

Lens capsular injury induced fibrosis was performed as described previously[41, 42]. Briefly, 6-8 weeks old male mice were anesthetized generally with intraperitoneal injection of pentobarbital sodium (70 mg/kg) and topically with dicaine eyedrop. After topical application of mydriatic, a small incision was made in the central anterior capsule of the right eye through the cornea with a 31-gauge hypodermic needle. The depth of injury was approximately 300 μm, which has been reported to form the fibrotic tissue around the lens puncture point. The mice were allowed to heal for 7 days. After that, the mice were sacrificed and the eyes were enucleated for the following experiments.

Lens epithelial tissue collection from cataract patients

A total of 27 cataract patients (age 17 to 81 yrs) with unilateral cataract presenting to the Depart of Ophthalmology, Army Medical Center, Army Medical University, participated in this study. Especially, the 17yrs patient suffered from traumatic cataract. Other patients have age related cataract. The parents provided informed consent to participate in the study and all samples were collected with written informed consent from the participants. The study protocol was approved by the ethics committee of Army Medical Center (No. 2018-31-32 and No. 2020-131). All procedures involving human material were performed in accordance with current ethical standards of the institutional and national research committee and with the Declaration of Helsinki ethical standards. All patients underwent detailed examination that included photography and slit-lamp microscopy of the lens. Lens epithelium samples were only from healthy patients. Abnormal coagulation function, etiological examination including hepatitis B, hepatitis C, syphilis, and human immunodeficiency virus, diabetes, hypertension, hyperlipidemia were excluded from the study.

Cell culture and EMT Induction

The human lens epithelial cell (SRA01/04) line was presented by Hao-Tian Lin from Zhong Shan Ophthalmic Center, Sun Yat-Sen University, as previously descripted [43].

SRA01/04 were grown in DMEM supplemented with 10% (vol/vol) FBS, 100 U/mL streptomycin, and 100 U/mL penicillin and grown at 37°C in a humidified incubator with 5% CO_2. Then LECs were seeded in 12-well cell culture plates at a concentration of 5.0×10^4 cells/mL and incubated in incubator (37°C and 5% CO_2) in standard medium for 24 h. Then LECs were treated with TGF-β2 (1 μg/mL) for 12h until the cell density grew to 60%. Next, the LECs were divided into different groups, to deal with pkm-in-1 or dasa-58 separately for 24h.

Lens culture and treatment

All experimental procedures conformed to the ARVO Statement for the Use of Animals in Ophthalmic and Vision Research. Briefly, lens culture protocol was followed previous publication with some modification[44-46]. Briefly, lenses from one-month C57BL/6J mice were carefully removed using forceps and a pair of fine scissors, and maintained in 4ml serum-free DMEM/F12 medium, containing 0.1 mg/ml L-glutamine, 50 IU/ml penicillin and 50 mg/ml streptomycin. TGF-β2 was added to the culture medium at the final concentrations of 5 ng/ml. Culture medium was renewed every second day throughout the culture period. Lenses were cultured for up to 5 days and the images were captured by using a dissecting microscope (Olympus, Japan).

Immunofluorescence staining

For mice, the eyeballs were removed and fixed in 4% PFA for 3h, then dehydrated in a sucrose solution (30%) for 3h. After that, eyeballs were embedded in OCT Tissue Tek Medium, and cut into 10-μm-thick sections adhered onto anti-slip slides by using a frozen section machine. For LECs, cells were grown on 13-mm coverslips in 24-well plates, and fixed in 4% PFA for 15 min at RT. Eyeballs sections and fixed LECs were washed with PBS, then samples were permeabilized and blocked in 0.3% Triton X-100 and 3% bovine serum albumin in PBS for 30 min at RT. After that, samples were incubated with appropriate primary antibodies (Table 1) overnight at 4◦C. After these steps, the samples were washed in PBS and incubated with the fluorescent secondary antibodies (Table 1) for 0.5 h at RT. And, samples were mounted after DAPI staining. In this process, samples were washed with PBS for 3 times/3min between each step. Images were captured with a confocal microscope.

Protein extraction and Western blot

Protein was were obtained from lens tissues in vivo experiments or primary cultured SRA01/04 in vitro. Samples were lysed in ice-cold lysis buffer, which consisted with RIPA and the protease inhibitor cocktail. Then, protein was clarified by heraeus sepatech and the supernatant was collected in new tubes. Then the concentrations of protein were determined by BCA Protein Assay kit. Loading buffer was added in

protein, and the mixture were boiled for 10min, and stored at -80°C.

For Western blot, twenty micrograms of total protein were used to separate on 10% SDS-polyacrylamide gels, and transferred to the polyvinylidene fluoride membranes. The membranes were blocked for 2h in Tris-buffered saline (TBS) with 5% non-fat skimmed milk powder, at RT. Then, the membranes were probed with primary antibodies (Table 1) at 4°C for overnight, and probed by the secondary antibodies at RT for 1.5h. Last, the Images were captured by Western blot automatic exposure apparatus.

Co-immunoprecipitation (Co-IP)

Co-immunoprecipitation was performed as manual described. Briefly, after thoroughly resuspend, magnetized and washed, SureBeads (Biorad, 1614013) were resuspended wit 5 μg PKM1 (CST, D30G6) PKM2(CST, D78A4); PANK4 (CST, D8N2C) antibodies in final volume of 200 μl, respectively, and IgG as the control. Rotate 10 min at room temperature (RT). Magnetize beads and discard supernatant, followed by repeat wash with 1,000 μl PBS-T for three times. Total lysate (300μg) from WT and *Pank4*$^{-/-}$ mice lens epithelium was diluted into a final volume of 500 μL NP40 Lysis Buffer (Solarbio, N8032), and PMSF (Solarbio, P0100). Rotate for 1 hr at room temperature (RT). Magnetize beads and discard supernatant. Wash with 1,000 μl PBS-T, resuspend the beads thoroughly, magnetize beads and discard supernatant, repeat three times (3×). Before the last magnetization, transfer the resuspended beads to a new tube. Spin down all tubes for several seconds. Magnetize beads and aspirate residual buffer from the tubes Add 40 μl 1× Laemmli buffer (biorad,1610747) and incubate for 10 min at 70°C. Magnetize beads and move eluent to a new vial. Equal amounts of extracts were separated by SDS-PAGE, and then they were transferred onto nitrocellulose membranes and then blotted with specific Antibodies.

Wound healing assay

SRA01/04s were cultured in a 12-well plate. After cells were grouped and got the corresponding treatment. Then when cell density grew to 90%, a 10 μl pipette tip was used to make a straight scratch through the monolayers. In the following period, cells migrated into the wound surface. The scratch width was used to represent the migrating ability of SRA01/04s. After 24 h, the scratch width was measured in five randomly selected fields. Data presented are repeated three times.

ATP measurement

Intracellular ATP was determined by using an ATP assay kit as previously described[47]. Briefly, cells were lysed 5 minutes, and centrifuged at 12,000 g at 4°C for 5 minutes. Then supernatant was added to test plate pre-treated with ATP detection reagent. Luminescence was measured by using a microplate reader. And the remaining cells

lysate was measured with the BCA protein assay kit to determine the concentration of protein. Finally, ATP concentration was expressed as μmol/g protein.

mRNA-Sequence and bio-informative data analysis

Total RNA extraction, mRNA library construction, and RNA sequencing

Total RNA was extracted from the lens epithelial tissues using TRIzol (Invitrogen, Carlsbad, CA, USA) according to the previously described protocol[48, 49]. Briefly, after routine RNA extraction, 25-100μL of diethyl pyrocarbonate-treated water was added to dissolve the RNA. The first-strand cDNA was generated using random hexamer-primed reverse transcription, followed by second-strand cDNA synthesis. A-tailing mix and RNA index adapters were added for incubating for end repair. The cDNA fragments were amplified using PCR, and the products were purified using Ampure XP beads (Beckman Coulter) dissolved in EB solution. The product was validated using an Agilent 2100 bioanalyzer for quality control. The double-stranded PCR products were heated, denatured, and circularized by the splint oligo sequence to derive the final library. The single-strand circle DNA (ssCir DNA) was formatted as the final library. The final library was amplified with phi29 to prepare a DNA nanoball (DNB), with more than 300 copies. DNBs were loaded into the patterned nanoarray, and single-end 50-base reads were generated on an MGISEQ2000 sequencing platform. The mRNA sequencing was performed by Genetics Biotech Inc and Biowavelet Inc in Chongqing, China.

Identification of differentially expressed genes

The expression level of genes was calculated using Salmon (version 1.4.0). The heatmap was drawn using pheatmap (version 1.0.8). Essentially, differential expression analysis was performed using the DESeq2 (version 1.4.5) with Q-value ≤0.05. To gain insight into the change of phenotype, geneontology (GO, http://www.geneontology.org/) and KEGG (https://www.kegg.jp/) enrichment analyses of the annotated differently expressed genes were performed using Phyper (https://en.wikipedia.org/wiki/Hypergeometric_distribution) based on the hypergeometric test. The significant terms and pathways were corrected with Q-value with a rigorous threshold (Q-value ≤0.05) using the Bonferroni method.

Pyruvate detection

The PA levels were determined by pyruvate assay kit (Pyruvate Assay Kit (ab65342/K609-100), Abcam). PA content were evaluated by measuring the absorbance at 505 nm. and the concentration PA was calculated using the following formula (A is an abbreviation of absorbance): PA content (μmol/ml) = (A (sample) - A (blank)) / (A (standard) - A (blank)) × standard concentration (0.2 μmol/ml) / protein concentration of sample (mg/ml).

Seahorse measurement

Seahorse analysis has been performed as previously described[50]. The Oxygen Consumption Rate (OCR) and the extracellular acidification rate (ECAR) were determined using the Seahorse XF96 Extracellular Flux Analyzer through the Seahorse XF Mito Stress Test Kit and Seahorse XF Glycolysis Stress Test Kit. It's used to measure the dependence of cells on the oxidative metabolism or preferentially the glycolytic function in cells. LECs were counted and seeded in XF96 Seahorse® microplates with 10,000 cells per well. After cells were grouped and got the corresponding treatment. Then when cell density grew to 80%, cells were cultured in XF Assay Medium supplemented with 1 mM glutamine in order to assess ECAR, in XF Assay Medium supplemented with 2 mM glutamine in order to assess OCR. and cells were placed in a CO_2-free incubator with 37℃ for 0.5h. The plate was left to equilibrate in before being transferred to the Seahorse XF96 analyzer. The pre-hydrated cartridge was filled with the indicated compounds and calibrated for 30 min in the Seahorse Analyzer. All the experiments were performed at 37℃. Normalization to protein content was performed after each experiment. The Seahorse XF Report Generator automatically calculated the parameters from Wave data that have been exported to Graphpad.

Statistical analysis

Statistical analysis was performed by Graph pad prism software (version 8.4, GraphPad Software). Data were presented as mean ± SD. For comparison between two groups, student's t test was performed. For comparisons among more than two groups, one way ANOVA followed by Bonferroni's post hoc test was performed. All statistical tests were two-side. A $p<0.05$ was considered statistically significant. All experiments were carried out at least three times unless otherwise stated.

Results

PANK4 levels increase with age in both rodent and human lens epithelium

PCO related fibrosis is reported associating with the aging process of lens epithelium[12]. In our study, we measured the expression levels of PANK4 in collected lens epithelium from different age-stages in human (from 17yrs old to 81yrs) and in mice (postnatal 15day (P15), 2-month old (2Mo), 6Mo and 12Mo). The intensity of fluorescence analysis reveals the expression patterns of PANK4 in lens epithelium at different age stages (Fig. 1A). It was found the levels of PANK4 increased gradually in parallel with the elevated aging stages (Fig. 1A). PANK4 puncta are specifically located in the cytoplasm of lens epithelium presented from 17yrs, 47yrs and 81yrs patients (Fig. 1A). To evaluate the distribution of the puncta, we outline the tangential plane of LEC with ImageJ software, thus quantified the gray value of the intensity of the fluorescence of which 47- and 81-yrs groups exhibit more intensive gray value in the cytoplasm (Fig.

316 1B). Furthermore, an increased number of puncta was found in the intracellular
317 cytoplasm of LECs in aged groups compared with that in younger groups (Fig. 1C). To
318 verify the immune-intensity results, we collected and pooled lens epithelium from
319 patients at ages of 40-50 yrs, 50-60 yrs, 60-70 yrs and over 80yrs groups. The intensities
320 of PANK4 blots were elevated in parallel with the increasing of age (Fig. 1D). While in
321 mice, PANK4 is localized in the whole anterior lens epithelium and equator by
322 immunostaining (Fig. 1E). Amplified high power crops showed the PANK4 positive
323 signals in cytoplastic localization (Fig. 1E and F), which are in consistent with the
324 immunostaining suggesting the promising pattern of PANK4 in lens. We collected mice
325 lens epithelium tissues at P15, 2Mo, 6Mo and 12Mo. PANK4 was also found increased
326 dramatically in an age-dependent tendency (Fig.1H), which strengthen the tendency of
327 PANK4 in human. Meanwhile, the lens epithelial EMT related characteristic molecules
328 such as N-cadherin, collagen I and α-SMA, which were upregulated in an aging
329 dependent tendency (Fig. 1H). These data suggest PANK4 is correlated with age
330 dependent lens epithelium fibrosis.
331
332 **PANK4 is required for lens epithelium fibrosis and EMT**
333 TGF-β2 is the major isoform in the aqueous humor, acts as the predominant pathogenic
334 factor in the development of lens epithelium EMT[51, 52]. Owing to this, we inject
335 TGF-β2 in to the anterior chamber to induce the EMT. As expected, the expression
336 levels of N-cadherin, collagen I and α-SMA upregulated, consistent with previous
337 reports[2, 53, 54]. Meanwhile, PANK4 protein level elevated as well (Fig. 2A and B),
338 which suggested the TGF-β2 induced LEC EMT is correlated with PANK4 level, in
339 another word, addition of TGF-β2 contributed to PANK4 expression. We next
340 considered whether the PANK4 modification alter the EMT by using *Pank4*$^{-/-}$ mice. It
341 was noticed dramatic decrease levels of N-cadherin, collagen I and α-SMA in lens
342 epithelium of 2-month-old *Pank4*$^{-/-}$ mice (Fig. 2C and D). To illustrate whether PANK4
343 is required for aging related lens fibrosis, we detected 1-year-old WT and *Pank4*$^{-/-}$ mice.
344 Similarly, N-cadherin, collagen I and α-SMA were also inhibited when PANK4 was
345 deficient (Fig. 2E and F). To determine the loss-of-function effect of PANK4 in EMT
346 alleviation, we next set up lens fibrosis model by TGF-β2 injection into mice eye.
347 Compared with WT group, *Pank4*$^{-/-}$ mice showed dramatic decrease of N-cadherin,
348 collagen I and α-SMA with and without TGF-β2 injections (Fig. 2G and H). Alleviation
349 of lens fibrosis was either found in TGF-β2 injection groups and lens puncture groups
350 (Fig. 2I) compared with WT mice. Together, these results demonstrated that PANK4 is
351 required for lens epithelial EMT. To confirm the loss-of-function effect of PANK4, we
352 also used siRNA^{Pank4} to knockdown it in SRA01/04s. Here we tested 3 different siRNA
353 sequences (#274, #962 and #1114) of which #1114 showed sufficient almost 80%
354 inhibition of PANK4, while the other two siRNAs exhibited attenuated inhibition effect

of nearly 30% (Suppl Fig.1). After 48h interference of Pank4 mRNA, the levels of collagen I and α-SMA decreased remarkably to 33% and 30%, while N-cadherin reached to 41% reduction (Fig. 2J and K). These results were accompanied by a decrease in HLCs migration test (Fig. 2L and M) that siRNA^{Pank4} inhibit the migration rate of HLCs, while overexpression of PANK4 by Lenti virus-Pank4 accelerate the migration, which together suggested PANK4 implicating in HLC EMT process.

PANK4 increases the EMT of lens epithelium by regulating respiratory electron transport and OXPHOS

Although PANK4 is considered as a putative kinase in PANK family, all amniote PANK4s, including human PANK4, encode Glu138Val and Arg207Trp substitutions which are predicted to inactivate kinase activity [55], the exact role of it is still under consideration. To investigate the causative role and mechanisms of PANK4 in EMT, we screen the mRNAs of lens epithelium by RNA-seq in comparation of WT and *Pank4*$^{-/-}$ mice (n=4). Volcano analysis indicated UCP2 (Fig3A), a mitochondrial uncoupling protein that is an ion/anion transporter located in mitochondrial inner membrane, and has a crucial role in regulating oxidative stress, cellular metabolism, cell proliferation and cell death[56]. Among molecular function, cellular component and biological process, “collagen binding”, “growth cone” and “regulation of cell-cell adhesion” GO terms were enriched (Fig. 3B). To further elucidate the mRNA enrichment, we performed GSEA analysis and found “electron transport chain”, “respiratory electron transport” and “oxidative phosphorylation” were enriched in WT group, which demonstrate the potential role of PANK4 in negatively regulating the process of glycolysis. To verify this potentiation, we tested concentrations of pyruvic acid and ATP in control and siRNA^{Pank4} groups. Dramatic elevation of pyruvic acid was found when Pank4 was knocked down, but reduction of ATP was observed compared with siControl group (Fig 3D). To test the transformation of OXPHOS to glycolysis by PANK4, we used Seahorse real-time detection to measure the extracellular acidification rate (ECAR) when *Pank4* was knock down by siRNA^{Pank4}. No significant of basal respiration was found between the two groups, however, spare respiratory capacity and maximum respiration were decreased in siRNA^{Pank4} group. Non-mitochondrial oxygen consumption was found dramatically increased (Fig 3E). In addition, GSEA analysis showed an enrichment of “Glycolysis” gene cluster in *Pank4*$^{-/-}$ group (Fig. 3F). Meanwhile, ratio of glycolytic rate, glycolytic capacity and glycolysis were all significant increase when *Pank4* was knocked down (Fig. 3G). These evidences suggested the essential role of PANK4 in negatively regulating the glycolysis. To verify the glycolysis status of lens epithelium when PANK4 deficient, we tested HIF-1α, HIF-1β and HIF-2α which are typical cellular oxygen sensors. As expected, all three hypoxic sensors elevated dramatically in *Pank4*$^{-/-}$ mice (Fig 3H) which strengthen the

394 conclusion that PANK4 is a negative regulator in the shift of OXPHOS and glycolysis.
395 To investigate how deficiency of PANK4 contribute to the incline of glycolysis and
396 OXPHOS, we also tested acetyl CoA carboxylase (ACC) and found unexpected
397 elevations (Fig. 3I). To confirm the possible role of PANK4 in catalyzing CoA, we also
398 tested the production of CoA under WT and Pank4 knock-out conditions. Similarly as
399 reported previously[55], no significant difference of CoA was observed between the
400 two groups (Suppl Fig. 2) which suggested there is a putative alternative role of PANK4
401 in regulating EMT. Interestingly, the concentration of lactate was also increased in lens
402 epithelium but not in blood (Fig. 3J). Since ACC is the key enzyme in catalyzing the
403 step of acetyl-CoA+ATP to malonyl-CoA+ADP/Pi, and the evidence showed ATP level
404 was declined in *Pank4*$^{-/-}$ group (Fig3. D), we speculated the step exhaust amount of ATP.
405 Alternatively, to further confirm the bypass of pyruvate to lactate, we tested the levels
406 of PFKP, PFKB3, LDHA, PDHK1 and PDH. No significant change was found in
407 PFKB3, PDHK1 and PDH, but levels of PFKP and LDHA were elevated (Fig. 3L and
408 M), which suggested an increasing activity of glycolysis, as the schematic diagram
409 indicated (Fig. 3N).
410
411 **PANK4 alters the balance of OXPHOS and glycolysis by negatively regulating**
412 **PKM2**
413 As PKM2 is considered as an associated protein that interact with rat PANK4 which
414 isolated from rat muscle cDNA library by yeast two-hybrid screening[30]. In addition,
415 by STRING protein-protein interaction networks functional enrichment analysis
416 (https://string-db.org/), we also found the potentiation relationship of PANK4 and PKM
417 with a score of 0.705. Seldom other evidence demonstrates the relationship between the
418 two molecules till now. Therefore, we use Co-IP to identify the potential binding
419 relationship between the two proteins. The blot results showed that PKM2 significantly
420 increased when immune-preciated binding with PANK4, while PKM1 not. To verify
421 the binding relationship of them, we used PKM2 antibody to bait the protein, which
422 show significant PANK4 immunoprecipitation (Fig 4A), indicating the promise
423 functional binding relationship of PANK4 and PKM2. It was clearly indicated the
424 specific location of PKM2 in lens epithelium (Fig. 4B), and the co-staining pattern of
425 PKM2 and PANK4 in cytoplasm of lens epithelial cells (Fig. 4C). We then ask the
426 regulation mechanism of them by using *Pank4*$^{-/-}$ mice, which demonstrated a significant
427 elevated level of PKM2 in lens epithelium and equator by immunostaining (Fig.4E and
428 F) as well as Western blot results (Fig.4G and H), with no significant difference of
429 PKM1 expression between WT and *pank4*$^{-/-}$ groups. By siRNA^{Pank4} knockdown of
430 *Pank4* mRNA in HLE cells, we also noticed the remarkable increase of PKM2 in
431 cytoplasm (Fig.4I), in consistent with the consequence of genome deficiency of pank4
432 in lens epithelium (Fig. 4D and E), following by a Western blot confirmation of elevated

PKM2 protein level without PKM1 significant change (Fig. 4J and K). With TGF-β2 injection induced lens epithelium fibrosis, deletion of *Pank4* increase the level of PKM2 as well (Fig. 4M and N), which suggested the negative regulation between PANK4 and PKM2. In subject of the conversion of phosphoenolpyruvate (PEP) to pyruvic acid, PEP is alternatively catalyzed by PKM2[57]. Strikingly, we found pyruvic acid increased when PANK4 was inhibited in LECs (Fig. 4L). These data suggested a potential novel role of PANK4-PKM2 axis in glycolysis in lens epithelium (Fig. 4M).

Inhibition of PKM2 attenuates EMT of lens epithelium by promoting the glycolysis related Warburg effect

The inhibition and activation of PKM2 by PKM-IN-1 and DASA-58, which are typical antagonist and agonist of PKM2, did not significantly change the PANK4 level which suggest the downstream role of PKM2. In presence of the PKM2 inhibition or activation by PKM-IN-1 or DASA-58, the levels of N-cadherin, collagen I and α-SMA increased when PKM2 inhibited, yet attenuated when activated, respectively and significantly (Fig. 5A and B). These results indicated an important role of PKM2 downstream the PANK4 in regulating the EMT of LECs. To confirm the downstream role of PKM2 which negatively regulated by PANK4, we used PKM-IN-1 to inhibit PKM2 elevation when PANK4 ablated. As expected, the expression of PKM2 was decreased but phosphor-PKM2 elevated, as well as the increased level of EMT markers, such as α-SMA, collagen I and N-cadherin (Fig. 5C). To understand the OXPHOS to glycolysis with EMT by PKM2 facilitation, we used Seahorse real-time detection to measure the mito-stress during the procedure (from 0 to 80 mins). Increase in extracellular acidification rate (ECAR) after adding glucose indicated the level of glycolysis of the cells, while a decrease in oxygen consumption rate (OCR) after adding oligomycin indicated the level of ATP production or OXPHOS of the cells. By DASA-58 treatment, glycolysis rate, glycolysis capacity and glycolysis reserve ECAR values were all decreased compared with *Pank4* knock down group (Fig. 5D and E). DASA-58 rescued the *Pank4* knock down related ECAR value elevation. No difference of maximum respiration, basal respiration and ATP production were found between sipank4 and DASA-58+sipank4 groups, which suggested the potential glycolysis regulation of PANK4 via PKM2 (Fig. 5F, G and H). Conversely, OCR value of spare respiratory capacity was increased (Fig. 5F, G and H). Pyruvate acid concentration was declined by PKM-in-1 treatment while increased when treated with DASA-58 (Fig. 5I). ATP level decreased strikingly in DASA-58 treatment group, while did not in PKM-IN-1 group (Fig. 5I), which suggested DASA-58 is effective in shifting PKM2 dependent OXPHOS and glycolysis. These results above directly reflect the lower level of glycolytic activity of SRA01/04 by DASA-58 treatment, yet could be rescued by *Pank4* knock down. However, PKM-IN-1 did not effectively take function in both ECAR and

OCR analysis. Since the activation of PKM2 attenuate lens epithelial EMT phenotype, we tried injection of PKM-IN-1 into anterior chamber in a TGF-β2 induced lens epithelium fibrosis model. By slit lamp observation, we could see opaque anterior lens (fibrosis) in PKM-IN-1 treated group at 3d, however, transparent lens in Veh group (Fig. 5J), which revealed PANK4 deficiency dependent activation of PKM2 is a promising target in lens epithelial fibrosis inhibition via incline of OXPHOS to glycolysis (Fig. 5M).

PANK4 deficiency is responsible for PKM2 phosphorylation at Y105 and HIF-α1 activation

Since we found a PANK4 deficiency related PKM2 elevation, we ask further mechanisms. Previous studies indicated that cytoplasmic PKM2 functions with tetramer formation, whereas nuclear PKM2 functions with dimer/monomer formation which may provide a protein binding ability[58]. Here we firstly treated the protein without SDS to exhibit the status of PKM2 under PANK4 deletion result in increased expression of ~120-kDa complex and ~60-kDa band, corresponding to dimeric and monomict PKM2 (Fig 6A and B). Increased total PKM2 was found at both ~120-kDa and ~60-kDa, while no significant increase of it was found at ~240-kDa (Fig. 6C). Further, p-PKM2(Y105) exert no significant difference between WT and *Pank4*$^{-/-}$ groups, but p-PKM2(S37) indeed declined (Fig. 6D and E), which suggested all the relative elevation of t-PKM2 was due to phosphorylation of Y105 residue. To investigate the cellular locations of p-PKM2 (Y105 and S37), we performed immunofluorescence staining in WT and *Pank4*$^{-/-}$ lens epithelium. It was showed p-PKM2 (Y105) signals were mainly located in the nuclear of lens epithelial cell in WT group, but in the cytoplasm of *Pank4*$^{-/-}$ ones (Fig. 6F). Plot profile of immunofluorescence signal described the levels of p-PKM2 (Y105) in lens epithelium of WT and *Pank4*$^{-/-}$ groups (Fig. 6G). To investigate the location of p-PKM2 (Y105), a transection of single cellular profile was delineated (Fig. 6H), which strengthen the immunofluorescence results that p-PKM2 (Y105) was mainly located in cellular nuclear. Meanwhile, p-PKM2 (S37) immunofluorescence signals were found puncta-shape and located in the cytoplasm and nuclear of WT lens epithelial cells, however, less puncta were found in *Pank4*$^{-/-}$ mice. Plot profile analysis indicated lower levels of p-PKM2 (S37) OD values in both cytoplasm and nuclear (Fig. 6G). For a single lens epithelial cell, the curve indicated a typical lower level of p-PKM2 (S37) in nuclear of lens epithelial cell in *Pank4*$^{-/-}$ mice. Together, these results indicated a mechanism that PANK4 deficiency contribute to the elevations of dimer and monomer forms of p-PKM2 (Y105), but not S37 residue.

PKM2 was previously reported as a PHD3 stimulated coactivator for hypoxia inducible factor 1 (HIF-1) to favor the genes associated with glycolysis[59]. Tyrosine

phosphorylation of PKM2 at residue 105 inhibit the formation of a PKM2 tetramer by dislodging the FBP binding, which was demonstrated to be important for the Warburg effect in hypoxia and cancer[60]. To illustrate the relationship between PKM2 and HIF-1 signaling contributed to lens epithelial EMT procedure attenuation. We perform Co-IP to investigate why PANK4 deletion triggered the LEC to a relatively hypoxic condition. Interestingly, much more binding activity was showed in WT lens epithelium rather than that of *Pank4*$^{-/-}$ mice (Fig. 6L), which demonstrated that PKM2(Y105) is physically interact with HIF-1α. However, no binding activity of PANK4 with HIF-1 was found in *Pank4*$^{-/-}$ mice (Fig. 6L). Numerous evidences reported aberrant EMT activator Zeb1 is the key factor for cell plasticity and promotes metastasis in kinds of cancers[61-63]. In response to the PKM2 upregulation and Y105-phospho form trans-nuclear activity, we speculate the p-PKM2 may correspondence to the HIF-1α and thus activate the transcription of EMT related transnuclear factors such as zeb1 and zeb2. To verify this hypothesis, we tested the mRNA levels of Zeb1 and Zeb2, which dramatically decreased in *Pank4*$^{-/-}$ group (Fig. 6M), which suggested a lower progression of EMT. To detail further potential signaling that has been affected by the PANK4 deletion, based on the RNAseq analysis, we noticed a relatively attenuation of Notch1 (Fig. 6N), which is one of the most important factors in leading epithelial EMT process, including lens fibrosis[51, 64]. Therefore, our results provided evidence that PANK4 is considered as a novel regulator of EMT in lens fibrosis. Deficiency of PANK4 contributed to the incline of lens epithelial cell glycolysis, with ATP exhaustion and thus HIF elevation. These results indicated deletion of PANK4 may contribute to the Warburg effect by alleviating pyruvate generation. We also found a relationship of PANK4 and PKM2 that the former negatively regulated PKM2 elevation and PKM2 dimer/monomer phosphorylation at Y105 residue. Both inhibition of PANK4 and activation of PKM2 by DASA-58 resulted in EMT process attenuation, which provide a promising potential target for lens fibrosis and PCO treatment.

Discussion

Cataract is the leading cause of blindness worldwide, tough it can be effectively cured by surgery, an EMT is central to fibrotic cataract[65]. In current study, we demonstrated that PANK4, which is the family member of PANK, is pivotal in LEC EMT process by regulating the balance of OXPHOS and glycolysis. We also found a potential and novel relationship between PANK4 and PKM2, and glycolysis related HIF elevation. Consequently, we propose a model for the regulation of PKM2 in response to PANK4. The PANK4 is strong enough to control LEC EMT process, whilst it was KO or KD, the typical EMT markers such as N-cadherin, collagen I and α-SMA were decreased, as well as the transcription factors that control the EMT process, like ZEB1, ZEB2.

PANK4 is located on chromosomes 1p36.32[66] and was firstly described as a

putative gene in type 2 diabetes in Chinese population[23]. High glucose could upregulate PANK4 in rat muscle from which was cloned[30]. However, 16 years later till then, limited literature investigated the further mechanism. We tried to collect diabetic patients' blood to exam the putative relationship between PANK4 and diabetes. Unfortunately, no significant difference of PANK4 mRNA level was seen (Suppl Fig. 3), which suggested PANK4 may not be a diabetic candidate gene. Interestingly, Liu's et al reported high PANK4 expression was more common in patients with poor-risk and complex karyotype and was an independent risk factor for event-free survival and overall survival [67], which need further demonstration. Due to the anti-apoptotic effect of PANK4, they speculated high level of PANK4 inhibit the pro-caspase-9, thus result in the shortage of patients' survival. In previous study, we generated a *Pank4*$^{-/-}$ mouse line by CRISPR/Cas9 system which showed increased number of apoptotic lens epithelial cells rather than WT group[22]. Therefore, PANK4 may have prominent anti-apoptotic role not only in pancreas, myeloid cells, but also in lens epithelium.

The human genome encodes three characterized pantothenate kinases (PANK1-3) plus a putative bifunctional protein PANK4 with a with a predicted amino-terminal Type II PANK domain and a carboxyterminal phosphatase domain (DUF89) which is large, diverse, and present in all domains of life[20, 68, 69]. DUF89 (Pfam01937) protein family occur as C-terminal fusions to pantothenate kinase (PanK) in plants, animals and chytrid fungi. Human PANK4 had activity against 4'-phosphopantetheine and its S-sulfonate or sulfonate was comparable to that against nitrophenyl phosphate (pNPP) [68]. However, Yao et al. described that all amniote PANK4s, including human PANK4, encode Glu138Val and Arg207Trp substitutions which are predicted to lack pantothenate kinase activity[55]. We firstly designed and generated *Pank4*$^{-/-}$ mice which have 5-bp mutation prior to exon 3 to get rid of the function PANK4. Interestingly, no significant difference of ac-CoA was found in lens between WT and *pank4*$^{-/-}$ mice, which demonstrated PANK4 may not involve in the pathway of CoA synthesis, namely lack the kinase activity. Nonetheless, GSEA analysis revealed noteworthy tendency of OXPHOS, electron transport chain, respiratory electron transport and ATP synthesis enriched in WT mice rather than in *Pank4*$^{-/-}$ mice (Fig 3A), which suggested the potential ability of PANK4 in redox regulation, independent of ac-CoA pathway.

With respect to Fang et al published papers, PKM2 was highlighted to be associated with PANK4 by the application of yeast two-hybrid system[30]. In current study, we discovered a novel regulation relationship between PANK4 and PKM2. When PANK4 loss it's function, PKM2 increased significantly which suggested a negative relation between them, without PKM1 was changed (Fig 4G). PKM2 controls the balance between energy production and the synthesis of metabolic precursors, thus has both metabolic and nonmetabolic functions, which are essential in the cytoplasm and nucleus, respectively. PKM2 with tetramer functions as a pyruvate kinase, whereas nuclear

PKM2 forms a dimer and functioning as a protein kinase[58], which interact with STAT3 to control downstream gene expression in SW480 cells. However, STAT3 and p-STAT3 were unchanged in lens epithelium of *Pank4*$^{-/-}$ mice by Western blot detection (Suppl Fig. 4), which suggested the nuclear dimeric PKM2 regulated nonmetabolic function intendent of classic STAT3 signaling. PKM2 activity is inhibited after phosphotyrosine binding through the release of FBP from the PKM2 allosteric pocket by Y105 phosphorylation which disrupt the tetrameric PKM2[60, 70]. We also noticed increased dimer and monomer forms of PKM2 under the PANK4 deletion, which indicate the glycolytic metabolic function was not likely due to the tetrameric PKM2. Thus, we speculate PKM2 not contribute to the glycolysis of LEC by tetramer formation under Pank4 ablation but involve in p-PKM2 related signaling transduction.

PKM2-dependent histone H3 modifications are instrumental in EGF-induced expression of cyclin D1 and c-Myc, tumor cell proliferation, cell-cycle progression, and brain tumorigenesis in its nonmetabolic functions of histone modification [71]. In our study, PKM2 dimer and monomer were increased, suggesting that metabolic activity of PKM2 is attenuated during LEC EMT. Thus, it is conceivable that the molecular interaction of PKM2 is highly context dependent, with cell fate determined by the form of PKM2 in regulating gene expression. In addition, PKM2 take essential role in Warburg regulation. Methylation of PKM2 activates aerobic glycolysis to promote tumorigenesis[29]. In transformed tumor cells, PKM2 are phosphorylated at Y105 by kinds of oncogenic kinases and dissociated to PKM2Y105 dimers which promote YAP nuclear translocation for tumor cell growth and transformation[72]. In our study, though the PKM2Y105 elevated dramatically when PANK4 loss of function, the total PKM2 increased at the same time which demonstrated the ratio of phosphorylation of Y105 vs total PKM2 protein consistent, in other words, the elevated PKM2 protein was phosphorylated at Y105. Meanwhile, we noticed the ratio of PKM2S37 *vs* total PKM2 decreased, but no significant change when *vs* inner control (Fig. 6A, B and C). In hepatocellular carcinoma cell lines, PKM2 could be phosphorylated at Ser37 by EGFR-activated ERK when stimulated with EGF, which promoted its nuclear translocation. Acting as both a serine/threonine protein kinase and a tyrosine protein kinase, PKM2 binds to and phosphorylates multiple transcription factors such as β-catenin and STAT3 in the nucleus to promote tumor-related gene transcription. And H3-Thr11 phosphorylation was dependent on the phosphorylation of PKM2 at Ser37[73]. Herein, to clarify whether PKM2S37 phosphorylate STAT3 under PANK4 deletion, STAT3 and p-STAT3 were both detected, but no change was observed (Suppl Fig. 4). Meanwhile, immunostaning of PKM2S37 in lens epithelium was attenuated in *Pank4*$^{-/-}$ group, which strengthen the conclusion that S37 residue related PKM2 transnuclear function may not involve in PANK4 unlocked PKM2 elevation.

The lens is sustained in a hypoxic environment in the eye without any vessel supply.

628 The oxygen partial pressure (pO_2) at the surface of the lens is 2.9 mm Hg, rather lower
629 than 24.1 mm Hg at the surface of the eye[74]. Thus, PKM2 activity contributes to a
630 high glycolytic potential to support lens metabolism [75-77]. It was indicated PKM2 is
631 capable of catalyzing the final rate-limiting step of glycolysis, which functioned as a
632 dimer to translocate into the nucleus, where it stimulates hypoxia-inducible factor 1α
633 (HIF-1α) transactivation domain function and recruitment of p300 to the hypoxia
634 response[59]. In current study, we found a novel phenomenon that HIF-1α and HIF-1β
635 increased dramatically in parallel with total PKM2 and PKM2Y105 elevation under the
636 PANK4 deletion. Current results showed a physical relationship of PKM2 and HIF-1α
637 in WT mice but dissociated in *Pank4*$^{-/-}$ group. Since lens epithelium in a hypoxic
638 environment in WT condition, PKM2 and HIF-1α may contribute to the homeostasis of
639 LEC survival and the balance of metabolism. Once the PANK4 was absent, more PKM2
640 were phosphorylated at Y105 residue and dissociated with HIF-1α, together with the
641 favor of glycolysis, suggesting a negative regulation loop of PANK4 on hypoxia. Even
642 though the *Pank4*$^{-/-}$ mice were housed in a high-level oxygen (70%) condition for
643 continuous 7 days, the HIF-1α were still elevated in the lens epithelium of *Pank4*$^{-/-}$ mice
644 (Suppl Fig. 5), which suggested HIF-1α elevation not only due to hypoxic condition,
645 but also could be regulated by PANK4. In normoxia condition, HIF-1α could be
646 hydroxylated in its C-terminal transcription activation domain by the arginyl
647 hydroxylase factor-inhibiting HIF (FIH)[78]. Oxygen dependent degradation of HIF-
648 1α is mediated by the hydroxylation of prolines 402 and 564 of human HIF-1α.
649 However, Warburg effect is capable of activating PI3K and Akt signaling to stabilize
650 the HIF-1α in an aerobic condition, which promote the pyruvate related glycolysis as
651 well[79]. Therefore, the consistent elevation of HIF-1α is depend on PANK4 deletion,
652 whatever in normoxia, hypoxia or hyperoxia conditions. Concerning the uncoupling
653 result of PKM2 and HIF-1α when PANK4 loss of function (Fig.6L), we speculate the
654 elevation of PKM2 and HIF-1α may take function in different ways rather than the
655 classic PKM2-HIF-1 positive feedback loop. PANK4 may functions as a coordinator
656 that organize PKM2 and HIF-1α in cellular OXPHOS and glycolysis activities. In
657 addition, we still cannot exclude the possibility that HIF-1α promote the PKM2 gene
658 transcription or PKM2 promote the HIF-1α gene transcription which need further
659 evidence. It was indicated in older animals, HIF-1α is necessary to maintain high level
660 of p27KIP1 which inhibiting the proliferation of LECs. In previous study, we also
661 discovered apoptotic phenotype of lens epithelial cell in *Pank4*$^{-/-}$ mice, which
662 strengthen the conclusion that PANK4 deficiency dependent HIF-1α elevation may
663 shed inhibition effect on the apoptosis and EMT of LECs.
664
665 **Figure Legends**
666 **Figure 1. PANK4 elevated with age and related to lens fibrosis and EMT.**

667 (**A**) Immunostaining of PANK4 in lens epithelium from patients aged at 17yrs, 47yrs
668 and 81yrs. The scale bar = 10μm. (**B**) Plot profile analysis of immunostaining in lens
669 epithelium of patients aged from 17yrs, 47yrs and 81yrs. (**C**) Quantification of PANK4
670 immunostaining positive puncta per cell in LECs, from patients aged at 17yrs, 47yrs
671 and 81yrs. (**D**) The levels of PANK4 protein in lens epithelium from cataract patients
672 (50-60yrs, 60-70yrs, 70-80yrs and more than 80yrs groups) were determined by
673 Western blotting assay and quantified by densitometry. (**E**) Immunostaining pattern of
674 PANK4 in the lens epithelium of adult mice. The scale bar = 200μm. HE image
675 presented an anatomy structure of lens. (**F**) and (**G**) High power images of PANK4
676 immunostaining results in anterior lens epithelium and equator of adult WT mice. The
677 scale bar = 10μm. (**H**) The levels of PANK4 protein in lens epithelium of from P15,
678 2Mo, 6Mo and 12Mo mice, detected by Western blotting assay and quantified by
679 densitometry. (**I**) The levels of N-cadherin, collagen I and α-SMA protein in lens
680 epithelium of from P15, 2Mo, 6Mo and 12Mo mice, detected by Western blotting assay
681 and quantified by densitometry. Results are expressed as means ± SD (n=15
682 independent cell for C; n=6 independent samples for D. n=4 independent experiments
683 for H and I). *$p < 0.05$ compared with 17yrs group in C; *$p < 0.05$ compared with 50-
684 60yrs group in D; *$p < 0.05$ compared with P15 group in H and I.
685
686 **Figure 2. PANK4 is required for lens epithelium fibrosis and EMT**
687 (**A**) and (**B**) The levels and quantifications of N-cadherin, collagen I and α-SMA protein
688 in WT lens epithelium after vehicle and TGF-β2 injection. (**C**) and (**D**) The levels and
689 quantifications of N-cadherin, collagen I and α-SMA protein in 2-month-old (2Mo) WT
690 and *Pank4*$^{-/-}$ lens epithelium. anti-PANK4 as positive control. (**E**) and (**F**) The levels
691 and quantifications of N-cadherin, collagen I and α-SMA protein in 12-month-old
692 (12Mo) WT and *Pank4*$^{-/-}$ lens epithelium. anti-PANK4 as positive control. (**G**) and (**H**)
693 The levels and quantifications of N-cadherin, collagen I and α-SMA protein in 2-month-
694 old (2Mo) WT and *Pank4*$^{-/-}$ lens epithelium, with and without TGF-β2 injection. (**I**)
695 Cultured lens with TGF-β2 (5.0ng/mL) addition for 2 and 4 days (solid arrow indicated
696 fibrosis in the lens). In vivo lens fibrosis phenotype, 7 days after puncture experiment
697 in WT and *Pank4*$^{-/-}$ mice. Observed and recorded by slit light microscope. (**J**) and (**K**)
698 The levels and quantifications of N-cadherin, collagen I, α-SMA and PANK4 protein
699 after siRNA administration. (**L**) and Lens epithelial cell migration assay at 0h, 12h and
700 24h, with Lenti virus-*Pank4* overexpression and siRNA interference treatments. (**M**)
701 Quantifications of the wound healing rate (%) at 0h, 12h and 24h. Results are expressed
702 as means ± SD (n=4 independent experiment for A-K; n=6 independent samples for L
703 and M). *$p < 0.05$ compared with 2-Mo WT group in B and D; *$p < 0.05$ compared
704 with 12-Mo WT group in F; *$p < 0.05$ compared with WT group, WT+ TGF-β2 group,
705 respectively, in H. *$p < 0.05$ compared with siPank4 group. *$p < 0.05$ compared with

706 Pank4 OE group, siPank4 groups, respectively, in M.
707
708 **Figure 3. EMT of lens epithelium by regulating respiratory electron transport and**
709 **OXPHOS**
710 (**A**) Volcano plot analysis of different expressed genes in lens epithelium in WT vs
711 *Pank4*$^{-/-}$ mice. (**B**) The most enriched GO terms of biological process, molecular
712 function and cellular component. (**C**) GSEA analysis enriched in electron transport
713 chain, oxidative phosphorylation and respiratory electron transport, showed positive
714 correlation with *Pank4*. (**D**) Concentrations of pyruvic acid and ATP in siControl and
715 si*Pank4* groups in lens epithelial cells. (**E**) Energy metabolism was analyzed on day 2
716 during reprogramming with the Seahorse instrument. Decrease in oxygen consumption
717 rate (OCR) after si*Pank4* was considered as the ATP production ability of the cells.
718 Spare respiratory capacity and maximum respiration were decreased, while non
719 mitochondrial oxygen consumption was increased after si*Pank4* treated. (**F**) GSEA
720 analysis enriched in electron transport chain, oxidative phosphorylation and respiratory
721 electron transport, showed negative correlation with *Pank4*. (**G**) Increase in
722 extracellular acidification rate (ECAR) after si*Pank4* treatment was considered as
723 glycolysis ability of the cells. (**H**) The Western blot results and the quantifications
724 indicated the protein levels of HIF-1α, HIF-1β and HIF-2α. (**I**) The protein level and
725 quantification of acetyl CoA carboxylase (ACC) in WT and *Pank4*$^{-/-}$ lens. (**K**)
726 Concentration of Acetyl-CoA (μM/L) in lens epithelium and (**L**) concentrations of
727 lactate (ng/μL) in blood and lens epithelium of WT and *Pank4*$^{-/-}$ mice. (**M**) The Western
728 blot results and the quantifications of PFKP, PFKB3, LDHA, PDHK1and PDH in WT
729 and and *Pank4*$^{-/-}$ lens. (**N**) Schematic illustration of current results. Results are
730 expressed as means ± SD (n=4 independent experiment for A-C, F; n=4 independent
731 experiment for D-M). *$p < 0.05$ compared with siPank4 group in D-G; *$p < 0.05$
732 compared with adult WT group in H-M.
733
734 **Figure 4. PANK4 negatively regulating PKM2 in lens epithelium**
735 (**A**) Co-IP results of PANK4 and PKM2. (B) Immunofluorescence staining results of
736 PKM2 in whole WT lens. PKM2 located in lens epithelium and equator. The scale bar
737 = 500μm. (**C**) Co-Immunofluorescence staining of PKM2 and PANK4 in lens
738 epithelium. The scale bar = 10μm. (**D**) and (**E**) Immunofluorescence staining of PKM2
739 in lens epithelium and equator of WT and *Pank4*$^{-/-}$ lens. The scale bar = 10μm (**F**) Plot
740 profile curve of PKM2 in WT and *Pank4*$^{-/-}$ lens. (**G**) and (**H**) Protein levels and
741 quantifications of PANK4, PKM1, PKM2 in WT and *Pank4*$^{-/-}$ lens. GAPDH as inner
742 control. (**I**) Immunofluorescence staining results of PKM2 in LECs in siControl group
743 and si*Pank4* group. The scale bar = 10μm (**J**) and (**K**) Protein levels and quantifications
744 of PANK4, PKM1, PKM2 in si-control group and siPank4 group. (**M**) and (**N**) Protein

levels and relative expression quantifications of PKM2 in lens epithelium of WT, WT with TGF-β2 injection, *Pank4*$^{-/-}$, *Pank4*$^{-/-}$ with TGF-β2 injection groups. (**L**) Concentrations of pyruvic acid (μg/ml) in LECs of negative control group, si-control group and siPank4 group. (**M**) Schematic illustration of current results. Results are expressed as means ± SD (n=4 independent experiment for G, H, J, K, M, N, L). Results are expressed as means ± SD (n=3 independent experiment for A-E). *p<0.05 compared with *Pank4*$^{-/-}$ group in H; *p < 0.05 compared with siControl group in K and L; *p<0.05 compared with WT, WT+TGF-β2, *Pank4*$^{-/-}$ group, respectively, in N.

Figure 5. **Negatively regulation of PKM2 by PANK4 attenuates EMT of lens epithelium by promoting the glycolysis related Warburg effect**

(**A**) and (**B**) Protein levels and quantifications of N-cadherin, α-SMA and collagen-I under PKM-IN-1 and DASA-58 treatments. GAPDH as inner control. (**C**) Protein levels and quantifications of p-PKM2, PKM2, N-cadherin, α-SMA and collagen-I under PKM-IN-1 inhibition in *Pank4*$^{-/-}$ mice. (**D**) and (**E**) Energy metabolism was analyzed on day 2 during Pank4 knockdown with the Seahorse instrument. Increase in extracellular acidification rate (ECAR) after si*Pank4* treatment was considered as glycolysis ability of the cells. Glycolysis, glycolysis capacity and glycolysis reserve were all increased, respectively, in si*Pank4* group rather than PKM-IN-1, DASA-58, PKM-IN-1+si*Pank4*, and DASA-58+si*Pank4* groups. (**F**) and (**G**) Decrease in oxygen consumption rate (OCR) after si*Pank4* was considered as the ATP production ability of the cells. Spare respiratory capacity elevated in si*Pank4* compared with PKM-IN-1, DASA-58 and PKM-IN-1+si*Pank4* groups, but decreased in comparison with DASA-58+si*Pank4* group. (**H**) Maximum respiration increased after si*Pank4* treatment compared with DASA-58 and DASA-58+si*Pank4* groups, while Proton leak increased after si*Pank4* treatment compared with PKM-IN-1, PKM-IN-1+si*Pank4* and DASA-58+si*Pank4* groups. ATP production was elevated in PKM-IN-1, DASA-58 and PKM-IN-1+si*Pank4* groups. (**I**) Concentration of pyruvic acid (μg/ml) increased in DASA-58 but decreased in PKM-IN-1 groups. Concentration of ATP (%) elevated both in Vehicle and PKM-IN-1 groups rather than that in DASA-58 group. (**J**) TGF-β2 injection with vehicle and PKM-IN-1 treatment in 2Month old *Pank4*$^{-/-}$ mice. (**M**) Scheme summarizing of current results. Results are expressed as means ± SD (n=4 independent experiment for A-I). Results are expressed as means ± SD (n=3 independent experiment for J). *p<0.05 compared with Vehicle (Veh) group in B and I; *p < 0.05 compared with si*Pank4* group in E, G, H.

Figure 6. **PANK4 deficiency is responsible for PKM2 Y105 phosphorylation and HIF-1α interaction with PKM2 Y105**

(**A**) Represented blot image of mice lens epithelium samples to show PKM2 monomer,

dimer and tetramer. (**B**) Relative expression of t-PKM2 vs GAPDH. (**C**) Analysis of relative OD values of WT PKM2 monomer, dimer and tetramer compared with that in *Pank4*$^{-/-}$ mice. (**D**) and (**E**) Levels of proteins and relative quantifications of p-PKM2(Y105), p-PKM2(S37) and t-PKM2 in WT and *Pank4*$^{-/-}$ mice lens epithelium. (**F**) Immunofluorescence staining of p-PKM2(Y105) in lens epithelium of WT and *Pank4*$^{-/-}$ mice. (**G**) Plot profile analysis described the level of p-PKM2(Y105) in WT and *Pank4*$^{-/-}$ mice lens epithelium. (**H**) Plot profile analysis of represented single lens epithelial cell immunofluorescence stained with p-PKM2(Y105). (**I**) Immunofluorescence staining of p-PKM2(S37) in lens epithelium of WT and *Pank4*$^{-/-}$ mice. (**J**) Plot profile analysis described the level of p-PKM2(S37) in WT and *Pank4*$^{-/-}$ mice lens epithelium. (**K**) Plot profile analysis of represented single lens epithelial cell immunofluorescence stained with p-PKM2(S37). (**L**) Co-IP was performed in WT and *Pank4*$^{-/-}$ mice lens epithelium. HIF-1α was physically interacted with PKM2, but dramatically dissociated when PANK4 ablated. (M) Relative mRNA levels of transcript factor Zeb1 and Zeb2, which decreased in *Pank4*$^{-/-}$ mice. (N) Transcriptional sequencing analysis of WT and *Pank4*$^{-/-}$ mice lens epithelium. (O) Scheme summarizing of the whole results. Results are expressed as means ± SD (n=4 independent experiment for B, E and M).

Supplementary Figure Legends

Figure 1. Screen assay of 3 types of designed siPank4.

Figure 2. Concentrations of acetyl-CoA in WT and *Pank4*$^{-/-}$ mice lens epithelium, brain cortex and retina.

Figure 3. Relative mRNA of Pank4 in healthy and diabetes patients.

Figure 4. Protein levels of total-Stat3 and phosphor-stat3 in WT and *Pank4*$^{-/-}$ mice lens epithelium.

Figure 5. Protein levels of PKM2 and HIF-1α in WT and *Pank4*$^{-/-}$ mice lens with and without 70% oxygen treatment for continuous 7 days.

Conflict of Interest Statement

All the authors declared that there is no conflict of interest.

Acknowledgement

We thank those heroes combating the 2019-nCov, especially Miss Ying Li and Juan Yu in our department, with respect. We also thank Prof. Lei Li from Shanghai Tech University for data evaluation. We thank our team members (Especially Jiao Hu) for their diligent work. The project is supported by National Natural Science Foundation of China (No. 82070945), Science and Technology Innovation Enhancement Project of Army Medical Center, Army Medical University (No. 2019CXJSB009 and No.

2019CXJSB021) and part grants from Basic Research and Scientific Frontier Foundation of Chongqing (cstc2019jcyj-msxmX0010).

References

1. Saika S, Yamanaka O, Sumioka T, Miyamoto T, Miyazaki K, Okada Y, Kitano A, Shirai K, Tanaka S and Ikeda K. Fibrotic disorders in the eye: targets of gene therapy. Prog Retin Eye Res. 2008; 27(2):177-196.
2. Eldred JA, Dawes LJ and Wormstone IM. The lens as a model for fibrotic disease. Philos Trans R Soc Lond B Biol Sci. 2011; 366(1568):1301-1319.
3. Piera-Velazquez S, Mendoza FA and Jimenez SA. Endothelial to Mesenchymal Transition (EndoMT) in the Pathogenesis of Human Fibrotic Diseases. J Clin Med. 2016; 5(4).
4. Wormstone IM. Posterior capsule opacification: a cell biological perspective. Exp Eye Res. 2002; 74(3):337-347.
5. Lovicu FJ and McAvoy JW. Structural analysis of lens epithelial explants induced to differentiate into fibres by fibroblast growth factor (FGF). Exp Eye Res. 1989; 49(3):479-494.
6. Saika S. Relationship between posterior capsule opacification and intraocular lens biocompatibility. Prog Retin Eye Res. 2004; 23(3):283-305.
7. Marcantonio JM, Syam PP, Liu CS and Duncan G. Epithelial transdifferentiation and cataract in the human lens. Exp Eye Res. 2003; 77(3):339-346.
8. Nagamoto T and Eguchi G. Morphologic compatibility or intraocular lens haptics and the lens capsule. J Cataract Refract Surg. 1997; 23(8):1254-1259.
9. Nagamoto T and Eguchi G. Effect of intraocular lens design on migration of lens epithelial cells onto the posterior capsule. J Cataract Refract Surg. 1997; 23(6):866-872.
10. Shu DY, Wojciechowski M and Lovicu FJ. ERK1/2-mediated EGFR-signaling is required for TGFbeta-induced lens epithelial-mesenchymal transition. Exp Eye Res. 2019; 178:108-121.
11. Shu DY and Lovicu FJ. Enhanced EGF receptor-signaling potentiates TGFbeta-induced lens epithelial-mesenchymal transition. Exp Eye Res. 2019; 185:107693.
12. Raghavan CT, Smuda M, Smith AJ, Howell S, Smith DG, Singh A, Gupta P, Glomb MA, Wormstone IM and Nagaraj RH. AGEs in human lens capsule promote the TGFbeta2-mediated EMT of lens epithelial cells: implications for age-associated fibrosis. Aging Cell. 2016; 15(3):465-476.
13. Roberts AB, Tian F, Byfield SD, Stuelten C, Ooshima A, Saika S and Flanders KC. Smad3 is key to TGF-beta-mediated epithelial-to-mesenchymal transition, fibrosis, tumor suppression and metastasis. Cytokine Growth Factor Rev. 2006; 17(1-2):19-27.
14. Swarup A, Bell BA, Du J, Han JYS, Soto J, Abel ED, Bravo-Nuevo A, FitzGerald PG, Peachey NS and Philp NJ. Deletion of GLUT1 in mouse lens epithelium leads to cataract formation. Exp Eye Res. 2018; 172:45-53.
15. Dahm R, van Marle J, Quinlan RA, Prescott AR and Vrensen GF. Homeostasis in the vertebrate lens: mechanisms of solute exchange. Philos Trans R Soc Lond B Biol Sci. 2011; 366(1568):1265-1277.
16. Casula M, Soranna D, Corrao G, Merlino L, Catapano AL and Tragni E. Statin use and risk of cataract: A nested case-control study within a healthcare database. Atherosclerosis. 2016; 251:153-158.
17. Leuschen J, Mortensen EM, Frei CR, Mansi EA, Panday V and Mansi I. Association of statin use

867 with cataracts: a propensity score-matched analysis. JAMA Ophthalmol. 2013; 131(11):1427-1434.
868 18. Dobrzynski JM and Kostis JB. Statins and Cataracts--a visual insight. Curr Atheroscler Rep.
869 2015; 17(2):477.
870 19. Zhang YM, Chohnan S, Virga KG, Stevens RD, Ilkayeva OR, Wenner BR, Bain JR, Newgard CB,
871 Lee RE, Rock CO and Jackowski S. Chemical knockout of pantothenate kinase reveals the metabolic
872 and genetic program responsible for hepatic coenzyme A homeostasis. Chem Biol. 2007;
873 14(3):291-302.
874 20. Hortnagel K, Prokisch H and Meitinger T. An isoform of hPANK2, deficient in pantothenate
875 kinase-associated neurodegeneration, localizes to mitochondria. Hum Mol Genet. 2003;
876 12(3):321-327.
877 21. Hong BS, Senisterra G, Rabeh WM, Vedadi M, Leonardi R, Zhang YM, Rock CO, Jackowski S
878 and Park HW. Crystal structures of human pantothenate kinases. Insights into allosteric regulation
879 and mutations linked to a neurodegeneration disorder. J Biol Chem. 2007; 282(38):27984-27993.
880 22. Sun M, Chen C, Hou S, Li X, Wang H, Zhou J, Chen X, Liu P, Kijlstra A, Lin S and Ye J. A novel
881 mutation of PANK4 causes autosomal dominant congenital posterior cataract. Hum Mutat. 2018.
882 23. Li Y, Wu GD, Zuo J, Meng Y and Fang FD. [Screening susceptibility genes of type 2 diabetes
883 in Chinese population by single nucleotide polymorphism analysis]. Zhongguo Yi Xue Ke Xue Yuan
884 Xue Bao. 2005; 27(3):274-279.
885 24. Xiang RL, Yang YL, Zuo J, Xiao XH, Chang YS and De Fang F. PanK4 inhibits pancreatic beta-
886 cell apoptosis by decreasing the transcriptional level of pro-caspase-9. Cell Res. 2007; 17(11):966-
887 968.
888 25. Zablocki GJ, Ruzycki PA, Overturf MA, Palla S, Reddy GB and Petrash JM. Aldose reductase-
889 mediated induction of epithelium-to-mesenchymal transition (EMT) in lens. Chem Biol Interact.
890 2011; 191(1-3):351-356.
891 26. Yadav UC, Ighani-Hosseinabad F, van Kuijk FJ, Srivastava SK and Ramana KV. Prevention of
892 posterior capsular opacification through aldose reductase inhibition. Invest Ophthalmol Vis Sci.
893 2009; 50(2):752-759.
894 27. Kinoshita JH and Nishimura C. The involvement of aldose reductase in diabetic complications.
895 Diabetes Metab Rev. 1988; 4(4):323-337.
896 28. WJ I, TL D, SM D, BP F, AM H, G B, J L, Y Y, M S, JW H, LN B, J X, MJ J, et al. PKM2 isoform-
897 specific deletion reveals a differential requirement for pyruvate kinase in tumor cells. Cell. 2013;
898 155(2):397-409.
899 29. F L, F M, Y W, L H, H Z, C J, Y W, P L, IM O, B L, G C, J J, S G, et al. PKM2 methylation by
900 CARM1 activates aerobic glycolysis to promote tumorigenesis. Nature cell biology. 2017;
901 19(11):1358-1370.
902 30. Li Y, Chang Y, Zhang L, Feng Q, Liu Z, Zhang Y, Zuo J, Meng Y and Fang F. High glucose
903 upregulates pantothenate kinase 4 (PanK4) and thus affects M2-type pyruvate kinase (Pkm2). Mol
904 Cell Biochem. 2005; 277(1-2):117-125.
905 31. Wong N, Ojo D, Yan J and Tang D. PKM2 contributes to cancer metabolism. Cancer Lett. 2015;
906 356(2 Pt A):184-191.
907 32. Li C, Zhao Z, Zhou Z and Liu R. PKM2 Promotes Cell Survival and Invasion Under Metabolic
908 Stress by Enhancing Warburg Effect in Pancreatic Ductal Adenocarcinoma. Dig Dis Sci. 2016;
909 61(3):767-773.
910 33. M X, Y Y, R K, S Z, L Y, L Z, X S, M Y, TR B, H W, L C, J J and D T. PKM2-dependent glycolysis

911 promotes NLRP3 and AIM2 inflammasome activation. Nature communications. 2016; 7:13280.
912 34. Qi W, Keenan HA, Li Q, Ishikado A, Kannt A, Sadowski T, Yorek MA, Wu IH, Lockhart S, Coppey
913 LJ, Pfenninger A, Liew CW, Qiang G, et al. Pyruvate kinase M2 activation may protect against the
914 progression of diabetic glomerular pathology and mitochondrial dysfunction. Nat Med. 2017;
915 23(6):753-762.
916 35. Liang J, Cao R, Zhang Y, Xia Y, Zheng Y, Li X, Wang L, Yang W and Lu Z. PKM2
917 dephosphorylation by Cdc25A promotes the Warburg effect and tumorigenesis. Nat Commun.
918 2016; 7:12431.
919 36. Yang W, Zheng Y, Xia Y, Ji H, Chen X, Guo F, Lyssiotis CA, Aldape K, Cantley LC and Lu Z.
920 ERK1/2-dependent phosphorylation and nuclear translocation of PKM2 promotes the Warburg
921 effect. Nat Cell Biol. 2012; 14(12):1295-1304.
922 37. Yang W, Xia Y, Ji H, Zheng Y, Liang J, Huang W, Gao X, Aldape K and Lu Z. Nuclear PKM2
923 regulates beta-catenin transactivation upon EGFR activation. Nature. 2011; 480(7375):118-122.
924 38. Yang W, Xia Y, Hawke D, Li X, Liang J, Xing D, Aldape K, Hunter T, Alfred Yung WK and Lu Z.
925 PKM2 phosphorylates histone H3 and promotes gene transcription and tumorigenesis. Cell. 2012;
926 150(4):685-696.
927 39. Lovicu FJ, McAvoy JW and de Iongh RU. Understanding the role of growth factors in
928 embryonic development: insights from the lens. Philos Trans R Soc Lond B Biol Sci. 2011;
929 366(1568):1204-1218.
930 40. Sun M, Chen C, Hou S, Li X, Wang H, Zhou J, Chen X, Liu P, Kijlstra A, Lin S and Ye J. A novel
931 mutation of PANK4 causes autosomal dominant congenital posterior cataract. Hum Mutat. 2019;
932 40(4):380-391.
933 41. Saika S, Kono-Saika S, Ohnishi Y, Sato M, Muragaki Y, Ooshima A, Flanders KC, Yoo J, Anzano
934 M, Liu CY, Kao WW and Roberts AB. Smad3 signaling is required for epithelial-mesenchymal
935 transition of lens epithelium after injury. Am J Pathol. 2004; 164(2):651-663.
936 42. Xiao W, Chen X, Li W, Ye S, Wang W, Luo L and Liu Y. Quantitative analysis of injury-induced
937 anterior subcapsular cataract in the mouse: a model of lens epithelial cells proliferation and
938 epithelial-mesenchymal transition. Sci Rep. 2015; 5:8362.
939 43. Wang R, Li J, Zhang X, Zhang X, Zhang X, Zhu Y, Chen C, Liu Z, Wu X, Wang D, Dongye M,
940 Wang J and Lin H. Extracellular vesicles promote epithelial-to-mesenchymal transition of lens
941 epithelial cells under oxidative stress. Exp Cell Res. 2021; 398(1):112362.
942 44. Chen X, Xiao W, Chen W, Luo L, Ye S and Liu Y. The epigenetic modifier trichostatin A, a
943 histone deacetylase inhibitor, suppresses proliferation and epithelial-mesenchymal transition of
944 lens epithelial cells. Cell Death Dis. 2013; 4:e884.
945 45. Hales AM, Chamberlain CG and McAvoy JW. Cataract induction in lenses cultured with
946 transforming growth factor-beta. Invest Ophthalmol Vis Sci. 1995; 36(8):1709-1713.
947 46. Hales AM, Chamberlain CG and McAvoy JW. Susceptibility to TGFbeta2-induced cataract
948 increases with aging in the rat. Invest Ophthalmol Vis Sci. 2000; 41(11):3544-3551.
949 47. Choi J, Seo BJ, La H, Yoon SH, Hong YJ, Lee JH, Chung HM, Hong K and Do JT. Comparative
950 analysis of the mitochondrial morphology, energy metabolism, and gene expression signatures in
951 three types of blastocyst-derived stem cells. Redox Biol. 2020; 30:101437.
952 48. Zhou JX, Liu YJ, Chen X, Zhang X, Xu J, Yang K, Wang D, Lin S and Ye J. Low-Intensity Pulsed
953 Ultrasound Protects Retinal Ganglion Cell From Optic Nerve Injury Induced Apoptosis via Yes
954 Associated Protein. Front Cell Neurosci. 2018; 12:160.

955 49. Zhang Z, Liu W, Huang Y, Luo L, Cai X, Liu Y, Ai L, Yan J, Lin S and Ye J. NLRP3 Deficiency
956 Attenuates Secondary Degeneration of Visual Cortical Neurons Following Optic Nerve Injury.
957 Neurosci Bull. 2020; 36(3):277-288.
958 50. Sun H, Yang X, Liang L, Zhang M, Li Y, Chen J, Wang F, Yang T, Meng F, Lai X, Li C, He J, He
959 M, et al. Metabolic switch and epithelial-mesenchymal transition cooperate to regulate
960 pluripotency. EMBO J. 2020; 39(8):e102961.
961 51. Chen X, Xiao W, Chen W, Liu X, Wu M, Bo Q, Luo Y, Ye S, Cao Y and Liu Y. MicroRNA-26a
962 and -26b inhibit lens fibrosis and cataract by negatively regulating Jagged-1/Notch signaling
963 pathway. Cell Death Differ. 2017; 24(8):1431-1442.
964 52. Allen JB, Davidson MG, Nasisse MP, Fleisher LN and McGahan MC. The lens influences
965 aqueous humor levels of transforming growth factor-beta 2. Graefes Arch Clin Exp Ophthalmol.
966 1998; 236(4):305-311.
967 53. Dawes LJ, Elliott RM, Reddan JR, Wormstone YM and Wormstone IM. Oligonucleotide
968 microarray analysis of human lens epithelial cells: TGFbeta regulated gene expression. Mol Vis.
969 2007; 13:1181-1197.
970 54. Lee JM, Dedhar S, Kalluri R and Thompson EW. The epithelial-mesenchymal transition: new
971 insights in signaling, development, and disease. J Cell Biol. 2006; 172(7):973-981.
972 55. Yao J, Subramanian C, Rock CO and Jackowski S. Human pantothenate kinase 4 is a pseudo-
973 pantothenate kinase. Protein Sci. 2019; 28(6):1031-1047.
974 56. Li J, Jiang R, Cong X and Zhao Y. UCP2 gene polymorphisms in obesity and diabetes, and the
975 role of UCP2 in cancer. FEBS Lett. 2019; 593(18):2525-2534.
976 57. Israelsen WJ and Vander Heiden MG. Pyruvate kinase: Function, regulation and role in cancer.
977 Semin Cell Dev Biol. 2015; 43:43-51.
978 58. X G, H W, JJ Y, X L and ZR L. Pyruvate kinase M2 regulates gene transcription by acting as a
979 protein kinase. Molecular cell. 2012; 45(5):598-609.
980 59. Luo W, Hu H, Chang R, Zhong J, Knabel M, O'Meally R, Cole RN, Pandey A and Semenza GL.
981 Pyruvate kinase M2 is a PHD3-stimulated coactivator for hypoxia-inducible factor 1. Cell. 2011;
982 145(5):732-744.
983 60. Hitosugi T, Kang S, Vander Heiden MG, Chung TW, Elf S, Lythgoe K, Dong S, Lonial S, Wang
984 X, Chen GZ, Xie J, Gu TL, Polakiewicz RD, et al. Tyrosine phosphorylation inhibits PKM2 to promote
985 the Warburg effect and tumor growth. Sci Signal. 2009; 2(97):ra73.
986 61. Krebs AM, Mitschke J, Lasierra Losada M, Schmalhofer O, Boerries M, Busch H, Boettcher M,
987 Mougiakakos D, Reichardt W, Bronsert P, Brunton VG, Pilarsky C, Winkler TH, et al. The EMT-
988 activator Zeb1 is a key factor for cell plasticity and promotes metastasis in pancreatic cancer. Nat
989 Cell Biol. 2017; 19(5):518-529.
990 62. Mohammadi Ghahhari N, Sznurkowska MK, Hulo N, Bernasconi L, Aceto N and Picard D.
991 Cooperative interaction between ERalpha and the EMT-inducer ZEB1 reprograms breast cancer
992 cells for bone metastasis. Nat Commun. 2022; 13(1):2104.
993 63. Han Y, Villarreal-Ponce A, Gutierrez G, Jr., Nguyen Q, Sun P, Wu T, Sui B, Berx G, Brabletz T,
994 Kessenbrock K, Zeng YA, Watanabe K and Dai X. Coordinate control of basal epithelial cell fate
995 and stem cell maintenance by core EMT transcription factor Zeb1. Cell Rep. 2022; 38(2):110240.
996 64. Zhou J, Jain S, Azad AK, Xu X, Yu HC, Xu Z, Godbout R and Fu Y. Notch and TGFbeta form a
997 positive regulatory loop and regulate EMT in epithelial ovarian cancer cells. Cell Signal. 2016;
998 28(8):838-849.

65. Kalluri R and Neilson EG. Epithelial-mesenchymal transition and its implications for fibrosis. J Clin Invest. 2003; 112(12):1776-1784.
66. Zhou B, Westaway SK, Levinson B, Johnson MA, Gitschier J and Hayflick SJ. A novel pantothenate kinase gene (PANK2) is defective in Hallervorden-Spatz syndrome. Nat Genet. 2001; 28(4):345-349.
67. Liu Y, Cheng Z, Li Q, Pang Y, Cui L, Qian T, Quan L, Dai Y, Jiao Y, Zhang Z, Ye X, Shi J and Fu L. Prognostic significance of the PANK family expression in acute myeloid leukemia. Ann Transl Med. 2019; 7(12):261.
68. Huang L, Khusnutdinova A, Nocek B, Brown G, Xu X, Cui H, Petit P, Flick R, Zallot R, Balmant K, Ziemak MJ, Shanklin J, de Crecy-Lagard V, et al. A family of metal-dependent phosphatases implicated in metabolite damage-control. Nat Chem Biol. 2016; 12(8):621-627.
69. Tilton GB, Wedemeyer WJ, Browse J and Ohlrogge J. Plant coenzyme A biosynthesis: characterization of two pantothenate kinases from Arabidopsis. Plant Mol Biol. 2006; 61(4-5):629-642.
70. HR C, MG VH, N W, JM A and LC C. Pyruvate kinase M2 is a phosphotyrosine-binding protein. Nature. 2008; 452(7184):181-186.
71. W Y, Y X, D H, X L, J L, D X, K A, T H, WK AY and Z L. PKM2 phosphorylates histone H3 and promotes gene transcription and tumorigenesis. Cell. 2012; 150(4):685-696.
72. Zhou Z, Li M, Zhang L, Zhao H, Sahin O, Chen J, Zhao JJ, Songyang Z and Yu D. Oncogenic Kinase-Induced PKM2 Tyrosine 105 Phosphorylation Converts Nononcogenic PKM2 to a Tumor Promoter and Induces Cancer Stem-like Cells. Cancer Res. 2018; 78(9):2248-2261.
73. Niu J, Li W, Liang C, Wang X, Yao X, Yang RH, Zhang ZS, Liu HF, Liu FY, Pei SH, Li WQ, Sun H, Fang D, et al. EGF promotes DKK1 transcription in hepatocellular carcinoma by enhancing the phosphorylation and acetylation of histone H3. Sci Signal. 2020; 13(657).
74. Helbig H, Hinz JP, Kellner U and Foerster MH. Oxygen in the anterior chamber of the human eye. Ger J Ophthalmol. 1993; 2(3):161-164.
75. Cheng HM, Chylack LT, Jr. and Chien J. Control pyruvate kinase activity in the lens. Exp Eye Res. 1978; 27(1):39-44.
76. Cheng HM, Chylack LT, Jr. and von Saltza I. Supplementing glucose metabolism in human senile cataracts. Invest Ophthalmol Vis Sci. 1981; 21(6):812-818.
77. Banroques J, Gregori C and Schapira F. Aging of pyruvate kinase isozymes in rabbit lens. Exp Eye Res. 1978; 27(4):427-434.
78. Hewitson KS, McNeill LA, Riordan MV, Tian YM, Bullock AN, Welford RW, Elkins JM, Oldham NJ, Bhattacharya S, Gleadle JM, Ratcliffe PJ, Pugh CW and Schofield CJ. Hypoxia-inducible factor (HIF) asparagine hydroxylase is identical to factor inhibiting HIF (FIH) and is related to the cupin structural family. J Biol Chem. 2002; 277(29):26351-26355.
79. Semenza GL. HIF-1: upstream and downstream of cancer metabolism. Curr Opin Genet Dev. 2010; 20(1):51-56.

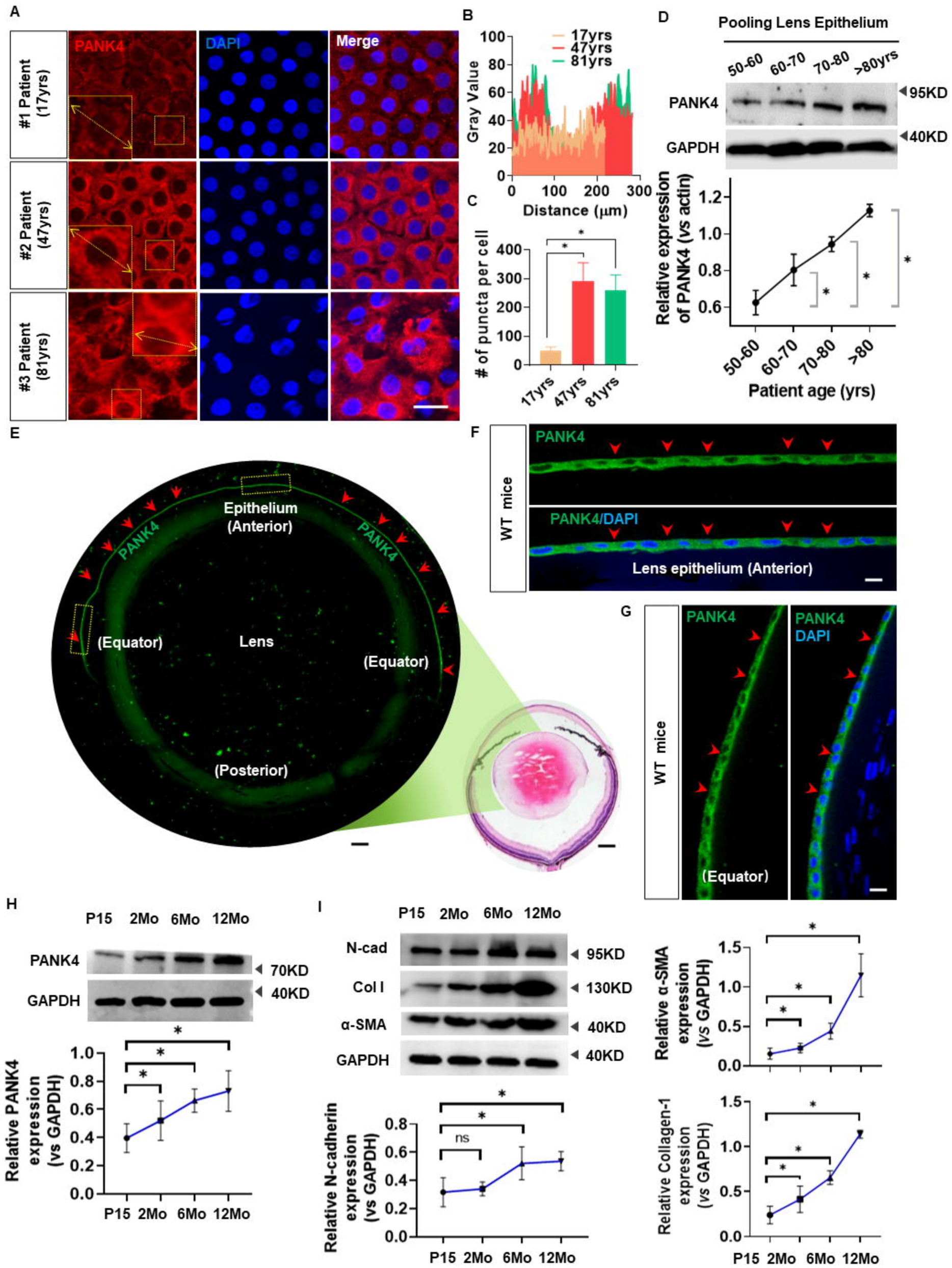
A
#1 Patient (17yrs)
#2 Patient (47yrs)
#3 Patient (81yrs)
PANK4
DAPI
Merge
B
17yrs
47yrs
81yrs
Gray Value
Distance (μm)
C
# of puncta per cell
17yrs
47yrs
81yrs
D
Pooling Lens Epithelium
50-60
60-70
70-80
>80yrs
PANK4
GAPDH
95KD
40KD
Relative expression of PANK4 (vs actin)
Patient age (yrs)
E
Epithelium (Anterior)
PANK4
(Equator)
Lens
(Posterior)
F
WT mice
PANK4
PANK4/DAPI
Lens epithelium (Anterior)
G
WT mice
PANK4
PANK4 DAPI
(Equator)
H
P15
2Mo
6Mo
12Mo
PANK4
GAPDH
70KD
40KD
Relative PANK4 expression (vs GAPDH)
I
N-cad
Col I
α-SMA
GAPDH
95KD
130KD
40KD
40KD
Relative N-cadherin expression (vs GAPDH)
ns
Relative α-SMA expression (vs GAPDH)
Relative Collagen-1 expression (vs GAPDH)

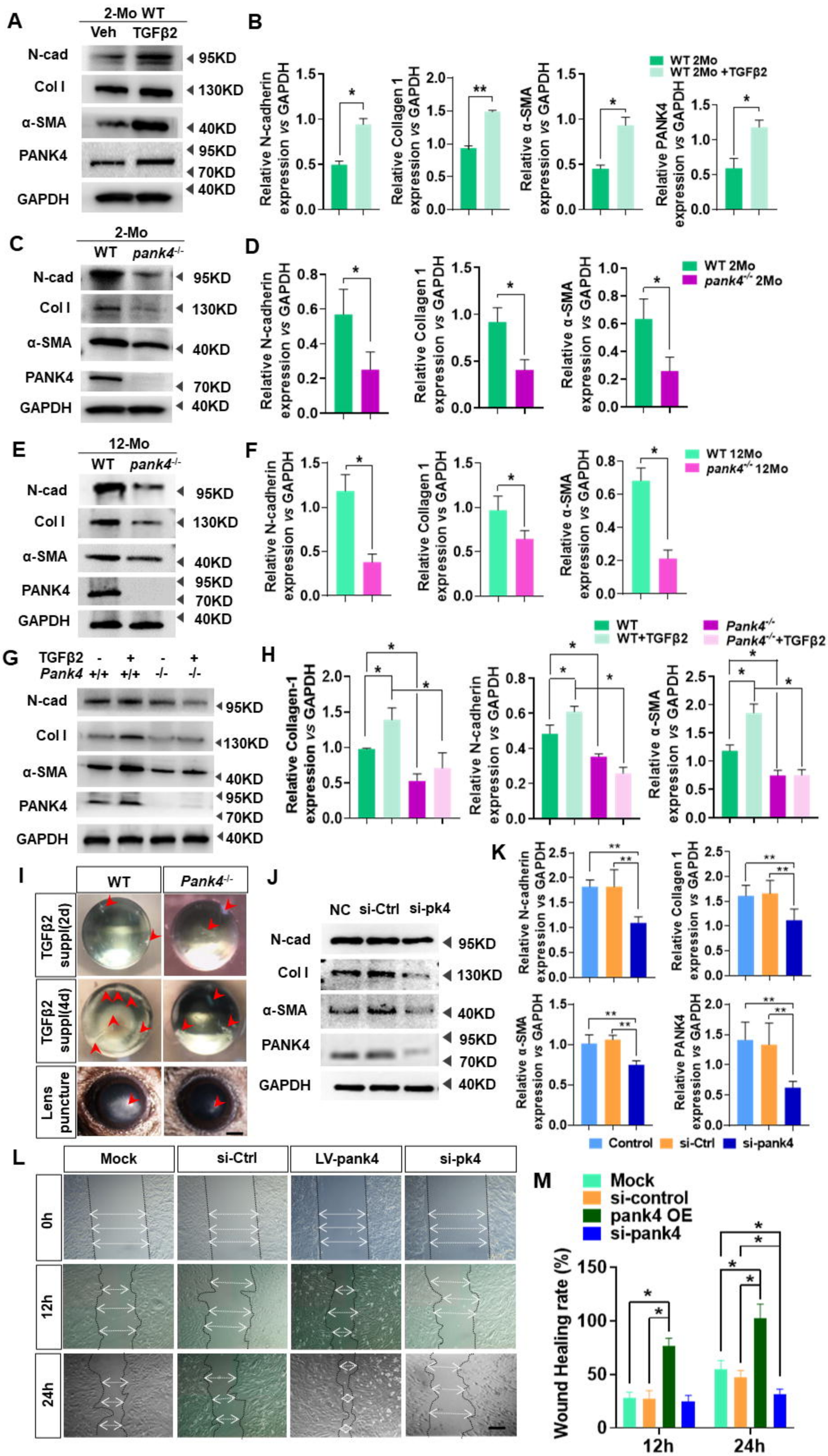
A
2-Mo WT
Veh
TGFβ2
N-cad
Col I
α-SMA
PANK4
GAPDH
95KD
130KD
40KD
95KD
70KD
40KD
B
Relative N-cadherin expression vs GAPDH
Relative Collagen 1 expression vs GAPDH
Relative α-SMA expression vs GAPDH
Relative PANK4 expression vs GAPDH
WT 2Mo
WT 2Mo +TGFβ2
C
2-Mo
WT
pank4-/-
D
WT 2Mo
pank4-/- 2Mo
E
12-Mo
F
WT 12Mo
pank4-/- 12Mo
G
TGFβ2
Pank4
H
WT
WT+TGFβ2
Pank4-/-
Pank4-/-+TGFβ2
I
TGFβ2 suppl(2d)
TGFβ2 suppl(4d)
Lens puncture
J
NC
si-Ctrl
si-pk4
K
Control
si-Ctrl
si-pank4
L
Mock
si-Ctrl
LV-pank4
si-pk4
0h
12h
24h
M
Mock
si-control
pank4 OE
si-pank4
Wound Healing rate (%)
12h
24h

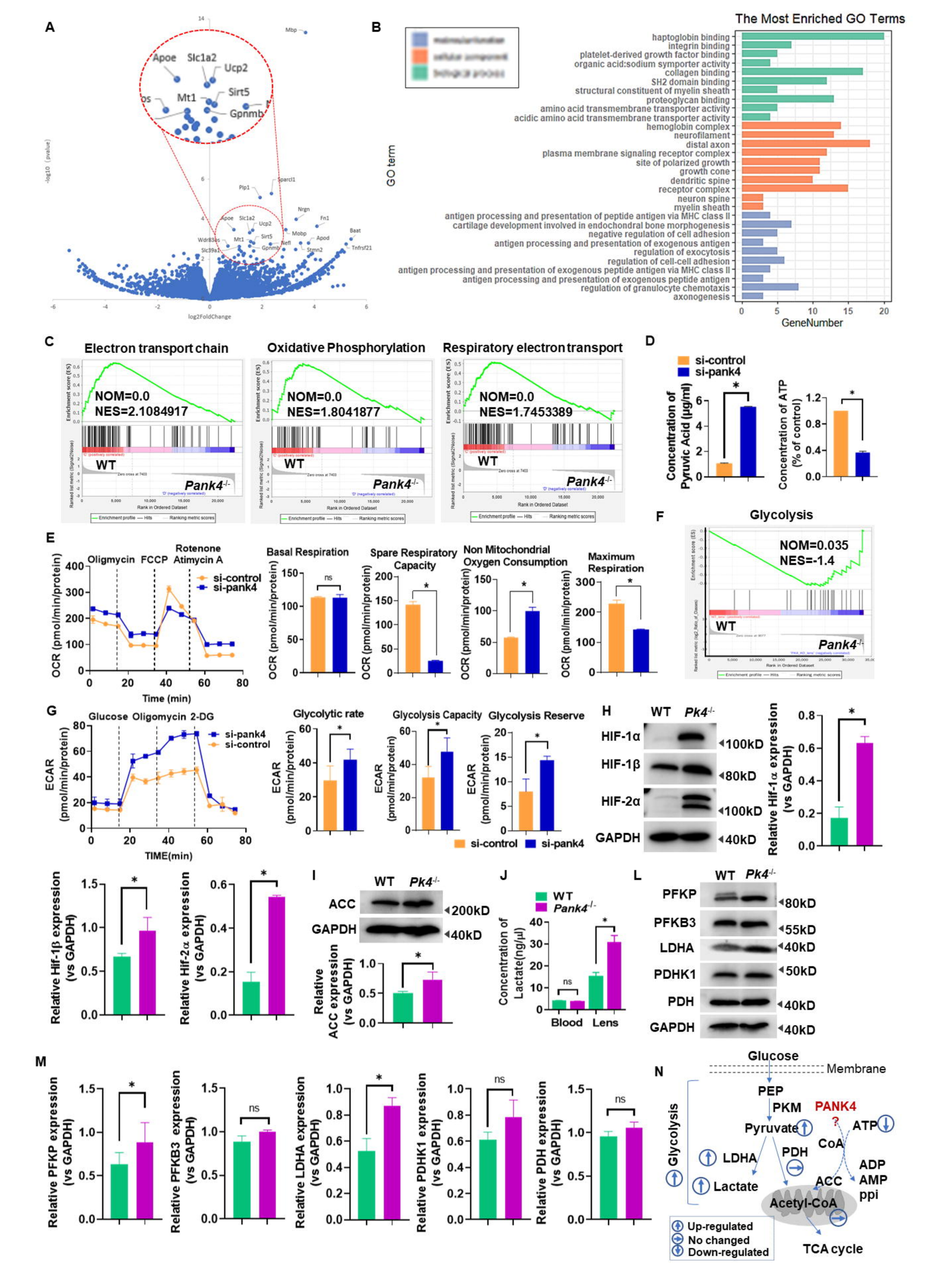
A
Apoe
Slc1a2
Ucp2
Sirt5
Mt1
Gpnmb
Mbp
Plp1
Sparcl1
Nrgn
Fn1
Mobp
Apod
Baat
Tnfrsf21
Stmn2
Nefl
Wdr83os
Slc39a1
-log10 (pvalue)
log2FoldChange
B
The Most Enriched GO Terms
GO term
haptoglobin binding
integrin binding
platelet-derived growth factor binding
organic acid:sodium symporter activity
collagen binding
SH2 domain binding
structural constituent of myelin sheath
proteoglycan binding
amino acid transmembrane transporter activity
acidic amino acid transmembrane transporter activity
hemoglobin complex
neurofilament
distal axon
plasma membrane signaling receptor complex
site of polarized growth
growth cone
dendritic spine
receptor complex
neuron spine
myelin sheath
antigen processing and presentation of peptide antigen via MHC class II
cartilage development involved in endochondral bone morphogenesis
negative regulation of cell adhesion
antigen processing and presentation of exogenous antigen
regulation of exocytosis
regulation of cell-cell adhesion
antigen processing and presentation of exogenous peptide antigen via MHC class II
antigen processing and presentation of exogenous peptide antigen
regulation of granulocyte chemotaxis
axonogenesis
GeneNumber
C
Electron transport chain
NOM=0.0
NES=2.1084917
Oxidative Phosphorylation
NOM=0.0
NES=1.8041877
Respiratory electron transport
NOM=0.0
NES=1.7453389
WT
Pank4-/-
D
si-control
si-pank4
Concentration of Pyruvic Acid (μg/ml)
Concentration of ATP (% of control)
E
Oligmycin
FCCP
Rotenone
Atimycin A
si-control
si-pank4
OCR (pmol/min/protein)
Time (min)
Basal Respiration
Spare Respiratory Capacity
Non Mitochondrial Oxygen Consumption
Maximum Respiration
ns
F
Glycolysis
NOM=0.035
NES=-1.4
WT
Pank4-/-
G
Glucose
Oligomycin
2-DG
si-pank4
si-control
ECAR (pmol/min/protein)
TIME(min)
Glycolytic rate
Glycolysis Capacity
Glycolysis Reserve
si-control
si-pank4
H
WT
Pk4-/-
HIF-1α
HIF-1β
HIF-2α
GAPDH
100kD
80kD
100kD
40kD
Relative Hif-1α expression (vs GAPDH)
Relative Hif-1β expression (vs GAPDH)
Relative Hif-2α expression (vs GAPDH)
I
WT
Pk4-/-
ACC
GAPDH
200kD
40kD
Relative ACC expression (vs GAPDH)
J
WT
Pank4-/-
Concentration of Lactate(ng/μl)
Blood
Lens
ns
L
WT
Pk4-/-
PFKP
PFKB3
LDHA
PDHK1
PDH
GAPDH
80kD
55kD
40kD
50kD
40kD
40kD
M
Relative PFKP expression (vs GAPDH)
Relative PFKB3 expression (vs GAPDH)
Relative LDHA expression (vs GAPDH)
Relative PDHK1 expression (vs GAPDH)
Relative PDH expression (vs GAPDH)
ns
N
Glucose
Membrane
PEP
PKM
PANK4
Pyruvate
ATP
CoA
LDHA
PDH
Glycolysis
Lactate
ACC
ADP
AMP
ppi
Acetyl-CoA
TCA cycle
Up-regulated
No changed
Down-regulated

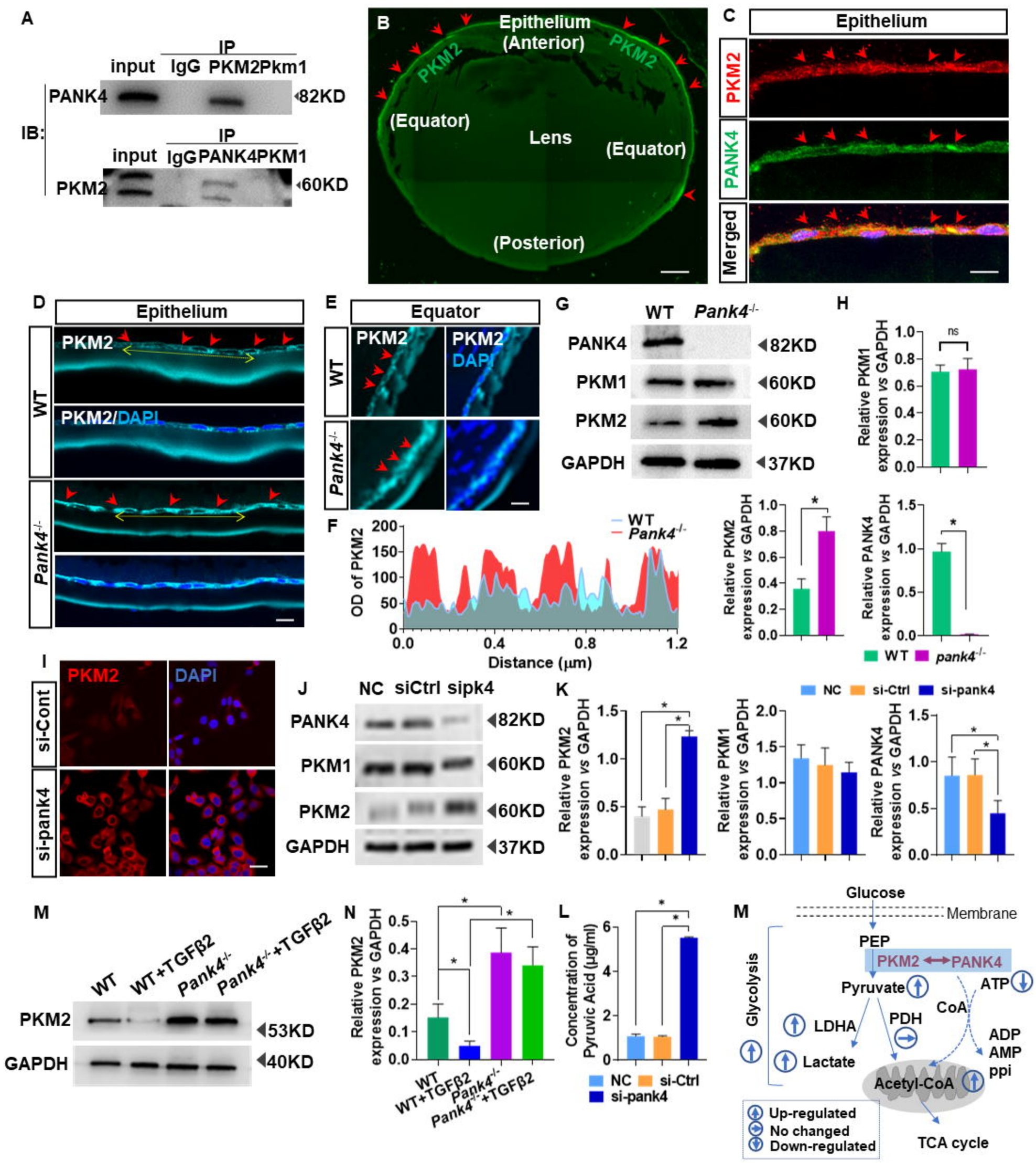
A
IP
input IgG PKM2Pkm1
PANK4
82KD
IB:
IP
input IgG PANK4PKM1
PKM2
60KD
B
Epithelium
(Anterior)
PKM2
PKM2
(Equator)
Lens
(Equator)
(Posterior)
C
Epithelium
PKM2
PANK4
Merged
D
Epithelium
WT
PKM2
PKM2/DAPI
Pank4-/-
E
Equator
WT
PKM2
PKM2
DAPI
Pank4-/-
G
WT Pank4-/-
PANK4
82KD
PKM1
60KD
PKM2
60KD
GAPDH
37KD
H
Relative PKM1 expression vs GAPDH
ns
Relative PKM2 expression vs GAPDH
Relative PANK4 expression vs GAPDH
WT pank4-/-
F
OD of PKM2
WT
Pank4-/-
Distance (μm)
I
si-Cont
si-pank4
PKM2
DAPI
J
NC siCtrl sipk4
PANK4
82KD
PKM1
60KD
PKM2
60KD
GAPDH
37KD
K
NC si-Ctrl si-pank4
Relative PKM2 expression vs GAPDH
Relative PKM1 expression vs GAPDH
Relative PANK4 expression vs GAPDH
M
WT
WT+TGFβ2
Pank4-/-
Pank4-/-+TGFβ2
PKM2
53KD
GAPDH
40KD
N
Relative PKM2 expression vs GAPDH
WT
WT+TGFβ2
Pank4-/-
Pank4-/-+TGFβ2
L
Concentration of Pyruvic Acid (μg/ml)
NC si-Ctrl
si-pank4
M
Glucose
Membrane
PEP
PKM2 PANK4
Pyruvate
ATP
CoA
LDHA
PDH
ADP
AMP
ppi
Glycolysis
Lactate
Acetyl-CoA
Up-regulated
No changed
Down-regulated
TCA cycle

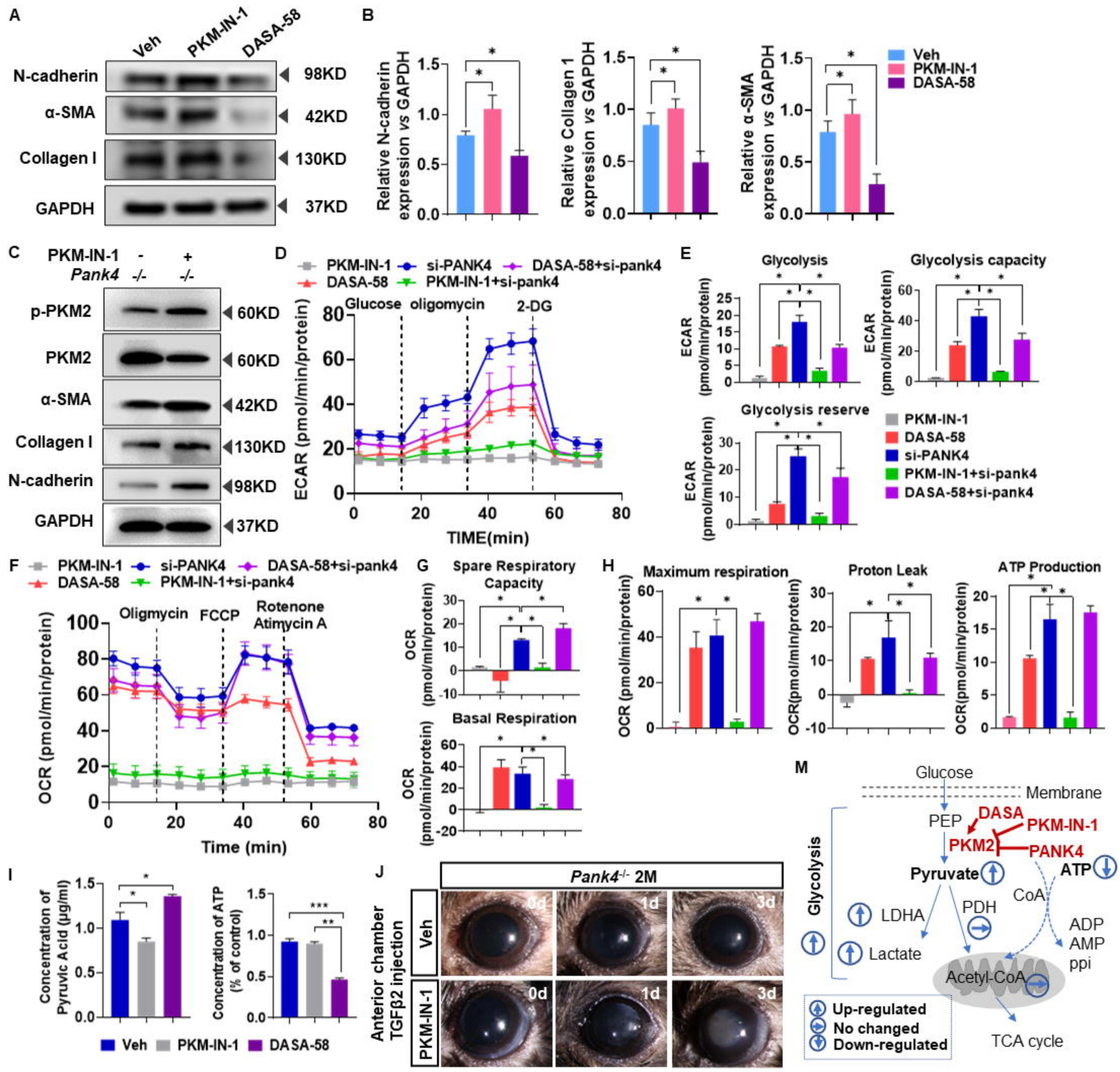
A
Veh
PKM-IN-1
DASA-58
N-cadherin
α-SMA
Collagen I
GAPDH
98KD
42KD
130KD
37KD
B
Relative N-cadherin expression vs GAPDH
Relative Collagen 1 expression vs GAPDH
Relative α-SMA expression vs GAPDH
Veh
PKM-IN-1
DASA-58
C
PKM-IN-1
Pank4
p-PKM2
PKM2
α-SMA
Collagen I
N-cadherin
GAPDH
60KD
60KD
42KD
130KD
98KD
37KD
D
PKM-IN-1
si-PANK4
DASA-58+si-pank4
DASA-58
PKM-IN-1+si-pank4
Glucose
oligomycin
2-DG
ECAR (pmol/min/protein)
TIME(min)
E
Glycolysis
Glycolysis capacity
Glycolysis reserve
ECAR (pmol/min/protein)
PKM-IN-1
DASA-58
si-PANK4
PKM-IN-1+si-pank4
DASA-58+si-pank4
F
PKM-IN-1
si-PANK4
DASA-58+si-pank4
DASA-58
PKM-IN-1+si-pank4
Oligmycin
FCCP
Rotenone
Atimycin A
OCR (pmol/min/protein)
Time (min)
G
Spare Respiratory Capacity
Basal Respiration
OCR (pmol/min/protein)
H
Maximum respiration
Proton Leak
ATP Production
OCR (pmol/min/protein)
I
Concentration of Pyruvic Acid (μg/ml)
Concentration of ATP (% of control)
Veh
PKM-IN-1
DASA-58
J
Pank4-/- 2M
Anterior chamber TGFβ2 injection
Veh
PKM-IN-1
0d
1d
3d
M
Glucose
Membrane
PEP
DASA
PKM-IN-1
PKM2
PANK4
Pyruvate
ATP
CoA
LDHA
PDH
Lactate
ADP
AMP
ppi
Acetyl-CoA
Glycolysis
Up-regulated
No changed
Down-regulated
TCA cycle

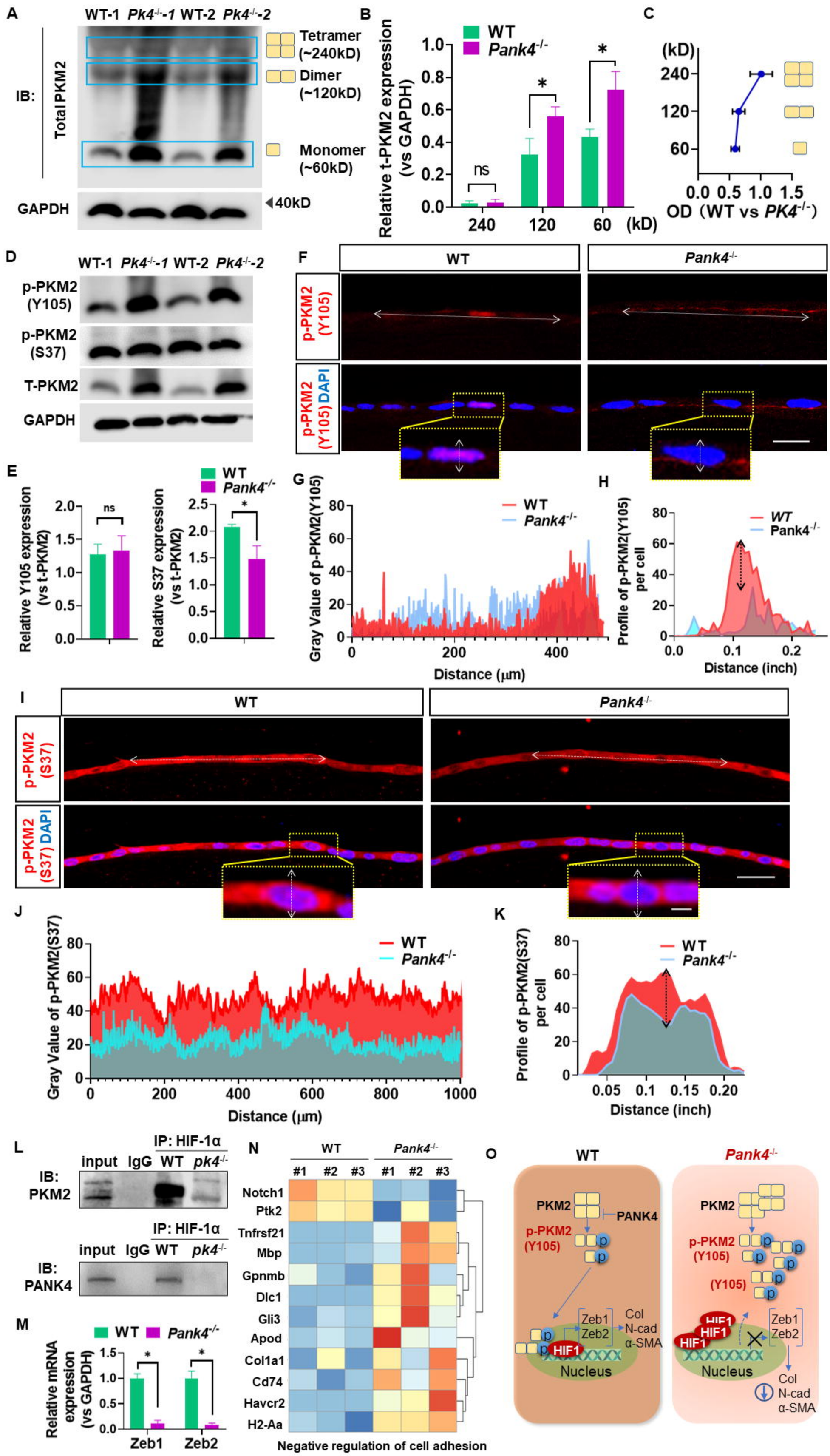
A
WT-1 Pk4-/--1 WT-2 Pk4-/--2
IB:
Total PKM2
Tetramer (~240kD)
Dimer (~120kD)
Monomer (~60kD)
GAPDH
40kD
B
WT
Pank4-/-
Relative t-PKM2 expression (vs GAPDH)
ns
*
240 120 60 (kD)
C
(kD)
240
120
60
0.0 0.5 1.0 1.5
OD (WT vs PK4-/-)
D
WT-1 Pk4-/--1 WT-2 Pk4-/--2
p-PKM2 (Y105)
p-PKM2 (S37)
T-PKM2
GAPDH
E
Relative Y105 expression (vs t-PKM2)
Relative S37 expression (vs t-PKM2)
F
WT
Pank4-/-
p-PKM2 (Y105)
p-PKM2 (Y105) DAPI
G
Gray Value of p-PKM2(Y105)
Distance (μm)
H
Profile of p-PKM2(Y105) per cell
Distance (inch)
I
p-PKM2 (S37)
p-PKM2 (S37) DAPI
J
Gray Value of p-PKM2(S37)
Distance (μm)
K
Profile of p-PKM2(S37) per cell
Distance (inch)
L
IP: HIF-1α
input IgG WT pk4-/-
IB: PKM2
IB: PANK4
M
Relative mRNA expression (vs GAPDH)
Zeb1
Zeb2
N
#1 #2 #3
Notch1
Ptk2
Tnfrsf21
Mbp
Gpnmb
Dlc1
Gli3
Apod
Col1a1
Cd74
Havcr2
H2-Aa
Negative regulation of cell adhesion
O
PKM2
PANK4
p-PKM2 (Y105)
HIF1
Zeb1
Zeb2
Col
N-cad
α-SMA
Nucleus